Contents lists available at ScienceDirect

Arabian Journal of Chemistry

journal homepage: www.ksu.edu.sa

Deciphering the healing power of *Swertia Chirayita*: A potential treatment for acute liver injury

Sa Guo [a], Cen Wu [a], Xinwei Liu [b], Xianli Meng [c], Yi Zhang [b,*], Shaohui Wang [b,d,**]

[a] State Key Laboratory of Southwestern Chinese Medicine Resources, School of Pharmacy, Chengdu University of Traditional Chinese Medicine, Chengdu 611137, China
[b] State Key Laboratory of Southwestern Chinese Medicine Resources, School of Ethnic Medicine, Chengdu University of Traditional Chinese Medicine, Chengdu 611137, China
[c] State Key Laboratory of Southwestern Chinese Medicine Resources, Innovative Institute of Chinese Medicine and Pharmacy, Chengdu University of Traditional Chinese Medicine, Chengdu 611137, China
[d] Meishan Traditional Chinese Medicine Hospital, Meishan 620010, China

ARTICLE INFO

Keywords:
Swertia chirayita
UPLC-Q-Exactive Orbitrap MS
Network pharmacology
Molecular docking
Acute liver injury

ABSTRACT

Acute Liver Injury (ALI), a highly prevalent liver disease in the last two decades, but there is still no effective treatment for it. As a member of Tibetan medicine, *Swertia chirayita* is commonly used for treating liver-related diseases, while the behavior of *S. chirayita* in CCl_4-induced ALI is deficient. In this work, the chemical constituents of *S. chirayita* were identified using a UPLC-Q-Exactive Orbitrap MS method. And the potential targets of the active compound of *S. chirayita* in CCl_4-induced ALI have been explored on the basis of bioinformatics analysis and ALI model. The findings revealed that a total of 49 compounds have been identified in *S. chirayita*, and 10 have been absorbed into blood as prototypes. Network pharmacology and molecular docking studies have shown that *S. chirayita* has a multi-component, multi-target profile for the treatment of CCl_4-induced ALI. Biochemical indicators testing demonstrated that Swertiamarine (STW) improved the levels of AST, ALT, MDA, SOD, TNF-α and IL-6 in CCl_4-induced ALI mouse model. Additionally, H&E staining indicated that STW significantly improved cellular necrosis, inflammatory infiltration, and other forms of pathological liver damage in mice. Meanwhile, quantitative reverse transcription PCR (qRT-PCR) showed that STW could ameliorate CCl_4-induced ALI by regulate the expression of EGFR, CASP3, STAT3 and other targets. In conclusion, as one of the active compounds of *S. chirayita*, STW could alleviate ALI by modulating the expression of biochemical indicators, liver pathological indicators and critical targets. This will provide a theoretical basis for the further research and development of the *S. chirayita*.

1. Introduction

Acute liver injury (ALI) is a common liver condition that is often caused by drug use, chemical exposure, or alcohol consumption. The main factors contributing to ALI are oxidative stress, inflammatory responses, necrosis, and apoptosis (Wu et al., 2021, Xin et al., 2021). Notably, carbon tetrachloride (CCl_4) is a well-known hepatotoxic substance frequently used in experimental models to induce both acute and chronic liver injury (Xiong et al., 2020). When CCl_4 is metabolized in a biological system, it produces harmful compounds like trichloromethyl radicals and peroxymethyl radicals, leading to an excess of superoxide dismutase and ultimately causing cellular necrosis, apoptosis, and liver damage (Di Paola et al., 2022, Wang et al., 2022a,b). Currently, synthetic drugs such as polyenyl phosphatidylcholine and

Abbreviations: ALI, Acute liver injury; ALT, Alanine aminotransferase; AMPK, Adenosine 5'-monophosphate (AMP)-activated protein kinase; AST, Aspartate aminotransferase; GO, Gene ontology; H&E, Hematoxylin and eosin; IL-6, Interleukin- 6; KEGG, Kyoto encyclopedia of genes and genomes; MDA, Malondialdehyde; qRT-PCR, Quantitative reverse transcription PCR; SOD, Superoxide Dismutase; STW, Swertimarin; TNF-α, Tumor necrosis factor-alpha; VEGF, Vascular endothelial growth factors.

* Corresponding author.
** Corresponding author at: State Key Laboratory of Southwestern Chinese Medicine Resources, School of Ethnic Medicine, Chengdu University of Traditional Chinese Medicine, Chengdu 611137, China.
E-mail addresses: 1057020534@qq.com (S. Guo), 1557659284@qq.com (C. Wu), lauxvv@163.com (X. Liu), xlm999@cdutcm.edu.cn (X. Meng), zhangyi@cdutcm.edu.cn (Y. Zhang), winter9091@163.com (S. Wang).

https://doi.org/10.1016/j.arabjc.2024.105930
Received 14 February 2024; Accepted 22 July 2024
Available online 23 July 2024

dicyclomine are commonly used to treat liver damage, but they can have unwanted side effects like gastrointestinal irritation and weight gain (Gawrieh and Chalasani 2015). Therefore, it is important to investigate natural products that may provide effective and less toxic alternatives to traditional treatments.

The study and utilization of natural products and biomolecules in promoting human health have been fundamental in medical and therapeutic sciences for centuries. These compounds, derived from a wide range of botanical, zoological, and microbiological sources, form the basis of traditional medicine (Hamza et al., 2020, Wang et al., 2022a,b). Modern pharmacognosy has brought scientific rigor to this field, revealing the intricate mechanisms through which these substances interact with biological pathways to provide health benefits (Xing et al., 2023). Biomolecules like phenolic compounds, alkaloids, terpenoids, and peptides are extracted from plants, animals, and microorganisms, demonstrating various pharmacological activities, including antioxidant, anti-inflammatory, antimicrobial, and anticancer effects (Amin 2008, Abdu et al., 2022, Bouabdallah et al., 2023, Du et al., 2023). Hence, natural products and biomolecules remain vital for the discovery and development of new health-promoting agents, emphasizing the ongoing pursuit of sustainable and effective medical treatments.

S. chirayita, a member of the *Swertia* L. of the gentianidae family, is widely used in Tibetan medicine and is mentioned in classic Tibetan medical texts such as *Jing Zhu Ben Cao* and *Si Bu Yi Dian* (He et al., 2022). Indigenous people utilized this medicinally important plant in a variety of ways. The whole plant directly or in decoction is traditionally used to cure inflammation, liver diseases, and digestive disorders. Juices made from different parts of this plant are used to treat malarial fevers, liver diseases and to stimulate the digestive tract (Swati et al., 2023). In addition, as a famous Tibetan medicinal product, Tibetan medicine considers *S. chirayita* to be a natural product with a bitter taste and cold nature, and prescription drugs containing *S. chirayita*, including ShiWei DiDa Capsule, ShiWuWei SaiErDou Pill and WuWei ZhangYaCai Tang-San, are commonly used clinically for the treatment of hepatitis, cirrhosis, hepatic fibrosis, and cholecystitis (Guo et al., 2023). Moreover, it contains various chemical constituents, including terpenoids, flavonoids, and organic acids, which contribute to its hepatoprotective effects. *S. chirayita*'s active ingredients, such as swertiamarin (STW), sweroside, and mangiferin, are commonly used in the treatment of liver diseases such as liver fibrosis, acute and chronic hepatitis, and hepatocellular carcinoma (Jaishree and Badami 2010). However, the specific role of *S. chirayita* in relation to CCl_4-induced ALI has not been extensively studied.

In 2007, Andrew L. Hopkins introduced the concept of network pharmacology, which aims to systematically understand the beneficial pathways and underlying mechanisms of biological agents and traditional Chinese medicines. This approach provides a framework to comprehend the complex interactions between multiple targets and diseases (Guo et al., 2021). Molecular docking, a technique used in computer-aided drug design, is also employed to validate network pharmacology predictions and has become an efficient research method in structural molecular biology (Mao et al., 2022). Both network pharmacology and molecular docking align with the holistic and evidence-based treatment principles of Chinese medicine, making them increasingly important in contemporary Chinese medicine research (Tang et al., 2016, Xie et al., 2021, Peng et al., 2023, Yang et al., 2023). However, there have been limited investigations applying these techniques to explore the role of *S. chirayita* in CCl_4-induced ALI.

In the present study, the main objectives were to identify the compounds present in *S. chirayita* and those absorbed into the bloodstream. And this was achieved this by using UPLC-Q-Exactive Orbitrap MS. Additionally, network pharmacology and molecular docking techniques was employed to identify the main targets and active compounds of *S. chirayita* in ALI. And the hepatoprotective effect of STW was also validated the in an ALI model. Finally, the key targets were confirmed using quantitative real-time polymerase chain reaction (qRT-PCR). Overall, these findings provide a solid foundation for further research on the enhancement and utilization of *S. chirayita*. A comprehensive diagram of our research methods is provided in Fig. 1.

2. Material and method

2.1. Chemicals and reagents

S. chirayita was sourced from Qinghai Jiumei Tibetan Medicine Pharmaceutical Co., Ltd (Qinghai, China) in 2022. Swertiamarin (STW), silymarin, loganic acid, chlorogenic acid, sweroside, isoorientin, and ursolic acid, all with a purity exceeding 98 %, were acquired from Lemeitian Pharmaceutical Technology Co., Ltd (Chengdu, China). CCl_4 was provided by Shanghai Yien Chemical Technology Co., Ltd (Shanghai, China), while isopropanol, chloroform and anhydrous ethanol were obtained from Chengdu Kelong Chemical Co., Ltd (Chengdu, China). Diagnostic tools included aspartate aminotransferase (AST) and alanine aminotransferase (ALT) kits from Jiangsu Edison Biotechnology Co., Ltd (Yancheng, China), a Superoxide Dismutase (SOD) kit courtesy of Beijing Box Biotechnology Co., Ltd (Chengdu, China), and a Malondialdehyde (MDA) kit procured from Biyuntian Biotechnology Co., Ltd (Shanghai, China). Tumor necrosis factor-alpha (TNF-α) and Interleukin-6 (IL-6) ELISA kits were obtained from Jiangsu Enzyme-free Biotechnology Co., Ltd (Yancheng, China). The Trizol reagent was purchased from Thermo Fisher ScientificThermo Fisher Scientific Co., Ltd (MA, US), and both the ABScript III RT Master Mix and qPCR Genious 2X SYBR Green Fast qPCR Mix were sourced from Wuhan Aibotech Biotechnology Co., Ltd (Wuhan, China). The names of the plants (*S. chirayita*) mentioned in the text have been verified through "World Flora Online" (http:/www.worldfloraonline.org) or MPNS (https://mpns.kew.org).

2.2. Analysis of the chemical composition of S. Chirayita

2.2.1. Preparation of S. chirayita extract

To extract the active compounds, 250 g of *S. chirayita* was subjected to two rounds of extraction with 2000 mL of 80 % ethanol under reflux for 90 min each. The resulting extracts were then combined, concentrated, and freeze-dried to yield the final *S. chirayita* extract.

2.2.2. Analysis of serum pharmacochemistry of S. chirayita

Sprague-Dawley rats (SCXK (Xiang) 2019–0004) were obtained from Hunan Slaughterhouse Laboratory Animal Co., Ltd (Changsha, China) and were housed at the Level III Laboratory of Pharmacology Research in Chinese Medicine (TCM-09–315) at Chengdu University of Traditional Chinese Medicine. The facilities were managed by the State Administration of Traditional Chinese Medicine and maintained a 12-hour day/night cycle with a consistent temperature of 24 ± 2 °C. The rats were fed standard chow (provided by Hunan Laboratory Animal Co., Ltd., Hunan, China) throughout the study.

Based on the clinical dosage of *S. chirayita* in humans (6–9 g/70 kg) (Swati et al., 2023), we calculated a dosage of 156 mg/kg for rats considering the acquisition rate of 80 % ethanolic extract from *S. chirayita* (23.07 %). To enhance the presence of chemical components, we increased the dosage to 1.56 g/kg for the test. The experimental procedure was as follows: after a seven-day adjustment period, the rats were randomly divided into two groups: a control group (treated with saline, 10 mL/kg) and a *S. chirayita* test group (administered an 80 % ethanolic extract of *S. chirayita*, 1.56 g/kg). The treatment was continued for seven more days through gavage. Prior to experimental blood sampling, the rats underwent a standard fasting period of 12 h with access to water. Blood samples were collected at specific time intervals after feeding: 5, 10, 15, 30, 45, 60, 90, 120, 240, and 480 min. These samples were then left at room temperature for one hour and centrifuged at 3500 r/min for 15 min at 4 °C. The clear top layer was stored at −80 °C. Following the completion of the treatment and blood

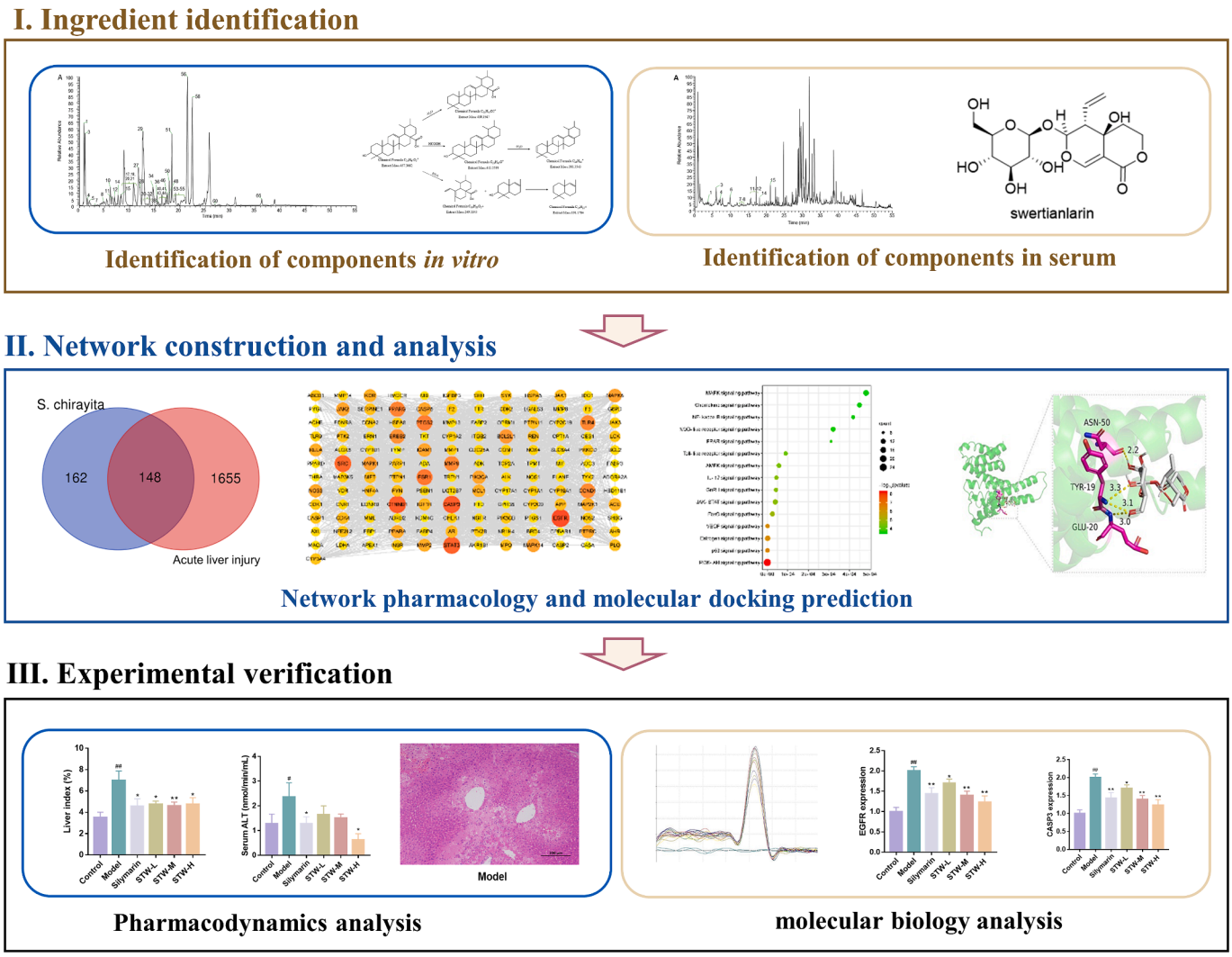

Fig. 1. The flowchart of this paper.

sampling process, all Sprague-Dawley rats were humanely euthanized in accordance with the guidelines provided by the American Veterinary Medical Association (AVMA) for the Euthanasia of Animals. The euthanasia protocol was part of our experimental design approved by the Animal Care and Use Committee at Chengdu University of Traditional Chinese Medicine, with the ethics approval number 2018–15, demonstrating our commitment to the ethics of animal research and the principles of 3Rs (Replacement, Reduction, and Refinement).

2.2.3. Preparation of UPLC-Q-Exactive Orbitrap MS analysis

First, the extract samples of *S. chirayita* was prepared for the study of chemical composition of it based on the method of UPLC-Q-Exactive Orbitrap MS. Briefly, to obtain a preparative concentration of 20 mg/mL of solubles, 20 mg of *S. chirayita* extract was added to a chromatographic grade methanol solution. Next, the serum samples (blank and *S. chirayita* groups) of SD rat were explored based on the means of serum pharmaceutical chemistry. Specifically, the blank serum or drug-containing serum sample were added to a 1:5 (v/v) acetonitrile solution for chromatography and obtained the supernatant through centrifugation. Next, 300 μL of chromatographic grade methanol was added to dissolve the serum sample. Finally, all samples were be filtered through a 0.22 μm membrane. Finally, the samples were analyzed using UPLC on a Vanquish model coupled to a Q-Exactive Orbitrap MS (Thermofisher, Waltham, MA, USA).

2.2.4. Chromatographic conditions

Sample separation was performed using a Waters XB-C18 column (100 mm × 2.1 mm, 1.7 μm) at a flow rate of 0.3 mL/min. The column temperature was maintained at 40 °C, and an injection volume of 2 μL was used. The mobile phase consisted of a 0.1 % aqueous formic acid solution (solvent A) and acetonitrile (solvent B). The elution gradient was programmed as follows: the proportion of solvent B was increased from 2 % to 10 % over 0–5 min, held at 10 % B from 5 to 10 min, gradually increased from 10 % to 65 % B between 10 and 30 min, further increased from 65 % to 95 % B during 30–45 min, and finally decreased from 95 % to 2 % B between 45 and 55 min.

2.2.5. Mass spectrometry conditions

A Q-Exactive Orbitrap mass spectrometer (MS) equipped with an electrospray ionization (ESI) feature was used to operate in both positive and negative ion modes. The specific parameters for data acquisition were set as follows: the spray voltage was maintained at 3500 V for both positive and negative ion modes; the ion transfer tube temperature was set at 320 °C, and the extra air heating temperature was set at 350 °C. The full MS resolution was set to 35,000, while the secondary mass spectral resolution was set to 17,500. The scan mass ranged from 100 to 1500 Da, and the collision energy gradient was set at 20, 40, and 60 Ev.

2.3. Network pharmacological analysis

2.3.1. Potential targets prediction

Using network pharmacological analysis, this study aimed to investigate the interaction between *S. chirayita* and ALI. Initially, the SwissTargetPrediction database (http:/www.swisstargetprediction.ch) was utilized to identify potential targets of the prototype blood components. Subsequently, ALI-related targets were gathered from the GeneCards (https://www.genecards.org/) and OMIM (https://omim.org/) databases. These targets were then standardized using the UniProt database (https: liww.uniprot.org/). Finally, Venn analysis (http://bioinfogp.cnb.csis.es/tools/venny/index.html) was performed to identify potential *S. chirayita* targets for ALI intervention.

2.3.2. Enrichment analysis

The Kyoto Encyclopedia of Genes and Genomes (KEGG) and Gene Ontology (GO) analytical tools were utilized to identify potential pathways associated with these common targets. Additionally, a protein–-protein interaction (PPI) network was created using the STRING database (http://string-db.org/) by inputting the relevant target genes.

2.4. Molecular docking analysis

ChemDraw 3D 20.0 software was used to illustrate the three-dimensional structures of the blood-absorbed compounds. The PDF files for the ten main targets were obtained from the PDB database (https://www.rcsb.org). The binding affinity of the prototype blood components to the top 10 key targets was then analyzed and visualized using AutoDock Vina software.

2.5. Analysis of the intervention of the STW in CCl_4-induced ALI

2.5.1. Animals and experimental design

Kunming mice were obtained from Beijing SPIFU Laboratory Animal Co., Ltd. (Beijing, China) and housed at the Level III Laboratory of Pharmacology Research in Chinese Medicine (TCM-09-315) at Chengdu University of Traditional Chinese Medicine, managed by the State Administration of Traditional Chinese Medicine. The mice were kept under a 12 h day/night cycle with a constant temperature of 24 ± 2 °C. After acclimating for 7 days, 54 mice were divided into six groups. The dosage for each group was determined based on references (Tian et al., 2014, Zhang et al., 2015) as follows: the Control group (received saline, 10 mL/kg daily), the Model group (also given saline, 10 mL/kg daily), the Silymarin group (received Silymarin, 0.2 g/kg daily), and low-, medium-, and high-dose STW groups (STW-L, 0.07 g/kg daily, STW-M, 0.14 g/kg daily and STW-H group, 0.28 g/kg daily respectively). These dosages were administered for 14 consecutive days. Two hours after the final dose, the Control group received an intraperitoneal injection of a peanut oil solution (10 mL/kg), while the rest of the groups were given intraperitoneal injections of 0.5 % CCl_4 mixed with the peanut oil solution (10 mL/kg). After 20 h, the blood samples were collected through the ophthalmic venous plexus. Additionally, the liver of each mouse was divided into two parts and stored in 4 % paraformaldehyde and −80 °C, respectively. The euthanasia protocol for mice followed the same procedure as described in section 2.2.2. The Chengdu University of Traditional Chinese Medicine Animal Use Committee approved all procedures, which were conducted in accordance with their guidelines.

2.5.2. Liver index analysis

The liver index is a commonly used metric in the field of toxicology, which measures the weight of an animal's liver relative to its total body weight. It is used to assess the severity of liver enlargement. The liver index is calculated using the formula: Liver index (%) = [Liver weight (g) / Mouse weight (g)] × 100. A higher liver index indicates a more severe case of hepatomegaly.

2.5.3. Biochemical analysis of the serum

The mice blood samples were collected into centrifuge tubes without heparin and sodium and allowed to coagulate at room temperature for an hour. Afterward, the samples were centrifuged at 3500 r/min for 15 min at 4 °C. The resulting serum samples were utilized to evaluate the concentrations of AST, ALT, TNF-α, and IL-6, following established protocols.

2.5.4. Biochemical analysis of the liver

Liver tissues from mice weighing 200 mg were homogenized with 1 mL of PBS buffer in a 1.5 mL centrifuge tube using a homogenizer set at 60 Hz for 90 s at 4 °C. This homogenization procedure was repeated four times. The homogenates were then centrifuged at 3500 r/min for 15 min at 4 °C. The supernatant was collected and used as the liver tissue homogenate sample. Subsequently, the levels of AST, ALT, MDA, and SOD in the liver tissue homogenates were measured following the manufacturer's instructions.

2.5.5. Histological analysis of the liver

For histopathological analysis, liver tissues were fixed in 4 % neutral formaldehyde and then stained with hematoxylin and eosin (H&E). The tissue samples were subjected to a series of steps, including gradient dehydration with ethanol, clarification, and embedding, before being sectioned. Microscopic images of the sections were captured using an Olympus microscope (Tokyo, Japan) after H&E staining.

2.5.6. Analysis of qRT-PCR

For the analysis of gene expression, total RNA was extracted from approximately 60 mg of liver tissue using Trizol reagent. The concentration and purity of the total RNA were measured with the Nanodrop Micro Nucleic Acid Analyzer (Thermo Fisher Scientific, USA). Subsequently, cDNA was synthesized from 1000 ng of total RNA, and a qRT-PCR reaction was performed on the Quantitative Real-Time Fluorescence PCR Detection System (Rocgene, Beijing, China). GAPDH was used as the reference gene to normalize RNA content. The primer sequences used for this process are provided in Table 1. The qPCR analysis parameters were set as follows: initial denaturation at 95 °C for 3 min, followed by 45 amplification cycles involving denaturation at 95 °C for 5 s, annealing at 55 °C for 30 s, and elongation at 72 °C for 60 s. The relative expression levels of the target genes were then calculated using the 2ˆ−Δ(ΔCt) method.

Table 1
qRT-PCR primer sequences in the liver of mice.

Genes	Primer	Sequences 5′–3′
EGFR	Forward primer	TTC AGC AAC AAC CCC ATC CTC TG
	Reverse primer	GCT TGG ATC ACA TTT GGG GCA AC
CASP3	Forward primer	TCA CTC GCG TTA ACA GGA AGG TG
	Reverse primer	TGA GCA TGG ACA CAA TAC ACG GG
CTNNB1	Forward primer	GGG TCC TCT GTG AAC TTG CTC AG
	Reverse primer	GGC ACC AAT GTC CAG TCC AAG AT
STAT3	Forward primer	GTC AGC AAT GGA GTA CGT GCA GA
	Reverse primer	GTT GGC GGG TCT GAA GTT GAG AT
SRC	Forward primer	TCC AGG CTG AGG AGT GGT ACT TT
	Reverse primer	CCA GCT TGC GGA TCT TGT AGT GT
ESR1	Forward primer	ATG CAC CAT TGA CAA GAA CCG GA
	Reverse primer	ACC CAT TTC ATT TCG GCC TTC CA
PTGS2	Forward primer	TCA GGT CAT TGG TGG AGA GGT GT
	Reverse primer	TCC TGC TTG AGT ATG TCG CAC AC
PPARG	Forward primer	TGC CAG TTT CGA TCC GTA GAA GO
	Reverse primer	CTC CCT GGT CAT GAA TCC TTG GC
TLR4	Forward primer	TCA TGG CAC TGT TCT TCT CCT GC
	Reverse primer	TAA GCC ATG CCA TGC CTT GTC TT
MMP9	Forward primer	AAA ACC TCC AAC CTC ACG GAC AC
	Reverse primer	CGC GGC AAG TCT TCA GAG TAG TT
GAPDH	Forward primer	GCC CAG AAC ATC ATC CCT GCAT
	Reverse primer	GCC TGC TTC ACC ACC TTC TTGA

2.5.7. Analysis of molecular dynamics

To further identify the key targets of STW for intervention in ALI, Molecular dynamics simulations including RMSD, RMSF, SARA, etc. of STW in complex with critical was performed using Gromacs2022 software. Specifically, Amber14sb was selected as the protein force field and Gaff2 was selected as the ligand force field.

2.5.8. Analysis of immunohistochemistry

Liver tissue sections were dewaxed and hydrated. Antigen repair was then performed in heated sodium citrate buffer. Closure was performed after removal of endogenous peroxidase. Finally, primary and secondary antibodies were incubated.

2.6. Statistical analysis

In this study, all data were analyzed using the GraphPad Prism 7.0 software through one-way analysis of variance (ANOVA). The values were reported as mean ± standard deviation. A p-value less than 0.05 was considered statistically significant.

3. Result

3.1. Analysis of chemical compounds of S. chirayita

S. chirayita has significant medicinal and developmental value. However, the specific medicinal substances it contains are not well understood. To address this, a comprehensive analysis of the *S. chirayita*'s phytochemical constituents was conducted using the UPLC-Q-Exactive Orbitrap MS technique. The result revealed the presence of 49 chemical constituents in the 80 % ethanol extract of *S. chirayita*, including 15 xanthones, 12 organic acids, 8 flavonoids, 6 iridoids, 4 phenylacetones, 3 terpenoids, and 1 fatty acids (Fig. 2, Supplementary Fig. S1, Supplementary Fig. S2 and Table 2). Additionally, the cleavage patterns of mangiferin, 1-Hydroxy-2,3,4,5-tetramethoxyxanthone, caffeic acid, isoorientin, and ursolic acid were elucidated, and described the identification process. Through this method, a total of 49 chemical components in *S. chirayita* was successfully identified.

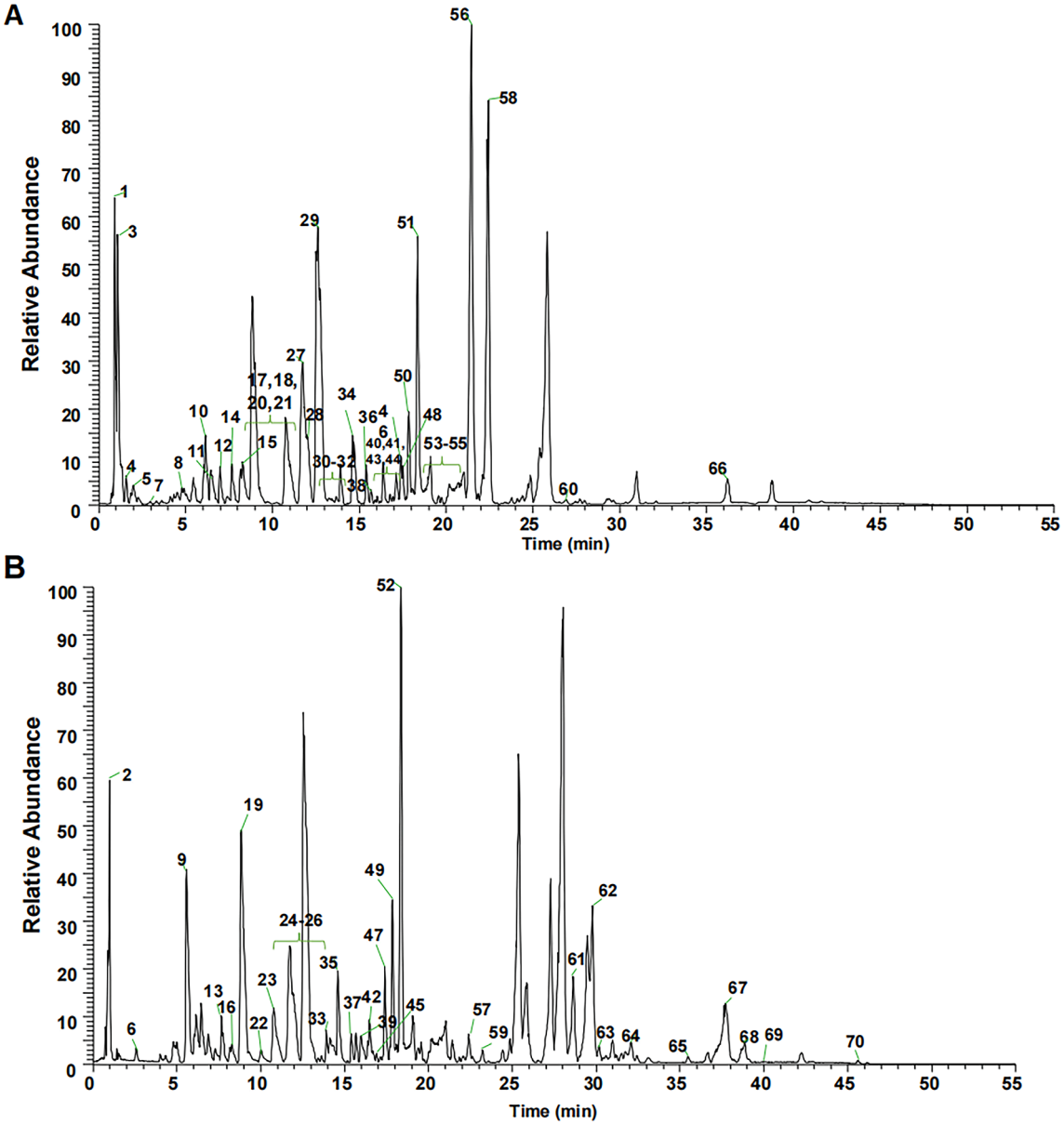

Fig. 2. TIC of 80 % ethanolic extract of *S. chirayita* in the negative (A) and positive (B) ion modes.

Table 2
Identification of chemical components of 80 % ethanolic extract of *Swertia chirayita* using UPLC-Q-Exactive Orbitrap MS.

No	tR/ min	Formula	Ion mode	Found at mass	Extraction mass	δ/ppm	Fragment ions	Compounds	Type	Ref
1	3.08	$C_7H_6O_5$	$[M-H]^-$	169.0142	169.0137	−2.96	125.0237 107.0132 97.0286 81.0336 69.0371	Gallic acid	Organic acids	(Zhao et al., 2018)
2	4.40	$C_{16}H_{24}O_{10}$	$[M-H]^-$	375.1297	375.1298	0.27	213.0766 151.0756 125.0595	8-Epiloganic acid	Iridoids	(Kucharska et al., 2017)
3	5.58	$C_{10}H_{12}O_2$	$[M+H]^+$	165.0910	165.0913	1.82	147.0807 137.0806 95.0498 91.0549 67.0550 55.0552	4-Phenylbutyric acid	Organic acids	(Kim et al., 2023)
4	6.69	$C_7H_6O_3$	$[M-H]^-$	137.0244	137.0237	−5.11	118.7628 109.0286 93.0337	3-Hydroxybenzoic acid	Organic acids	(Wang et al., 2015)
*5	7.04	$C_{16}H_{24}O_{10}$	$[M-H]^-$	375.1297	375.1298	0.27	213.0766 179.0558 169.0865 151.0756 125.0595 119.0340 113.0236	Loganic acid	Iridoids	(Tao et al., 2017)
6	7.33	$C_7H_6O_2$	$[M+H]^+$	123.0441	123.0443	1.63	95.0498 77.4372	p-Hydroxybenzaldehyde	Organic acids	(Wang et al., 2016)
7	7.55	$C_8H_8O_4$	$[M-H]^-$	167.0350	167.0345	−2.99	152.0110 123.0805 108.0211 95.0494 61.9312	Vanillic acid	Organic acids	(Liu et al., 2019)
*8	8.14	$C_{16}H_{18}O_9$	$[M-H]^-$	353.0878	353.0887	2.53	191.0559 161.0240 127.0394	Chlorogenic acid	Phenylpropanoids	(Deng et al., 2022)
*9	8.27	$C_{16}H_{22}O_{10}$	$[M+H]^+$	375.1286	375.1287	0.27	279.1593 213.0759 195.0656 177.0549 167.0704 149.0598	Swertiamarin	Iridoids	(Swati et al., 2023)
10	8.78	$C_7H_6O_4$	$[M-H]^-$	153.0193	153.0187	−3.92	125.0603 109.0653 108.9588 91.0549 81.0332	Protocatechuic acid	Organic acids	(Liu et al., 2019)
11	8.84	$C_{10}H_8O_3$	$[M+H]^+$	177.0546	177.0548	1.13	149.0601 121.0652 105.0704 103.0548	6-Hydroxy-4-methylycoumarin	Phenylpropanoids	(Kim et al., 2023)
12	8.85	$C_9H_6O_4$	$[M-H]^-$	177.0193	177.0188	−2.82	177.0189 149.027 133.0288 121.0289 105.0338 93.0336 81.0336	6,7-Dihydroxycoumarin	Phenylpropanoids	(Huang et al., 2021)
13	8.87	$C_7H_6O_4$	$[M-H]^-$	153.0193	153.0187	−3.92	109.0287 108.0209 91.0179 81.0336	Protocatechuate	Organic acids	(Kim et al., 2023)
14	10.20	$C_9H_8O_2$	$[M+H]^+$	149.0597	149.0600	2.01	131.0853 121.0653 107.0496 103.0548	Cinnamic acid	Organic acids	(Guan et al., 2019)
15	10.77	$C_{16}H_{20}O_9$	$[M-H]^-$	357.1180	357.1185	1.40	195.0656 177.0549 149.0600 121.0652	Gentiopicroside	Iridoids	(Zhang 2021)
*16	11.75	$C_{16}H_{22}O_9$	$[M-H]^-$	357.1191	357.1199	2.24	328.3954 257.5395 195.0661 177.0554 149.0237 125.0236	Sweroside	Iridoids	(Zhang 2021)
17	12.71	$C_{19}H_{18}O_{11}$	$[M-H]^-$	421.0776	421.0782	1.42	331.0463 301.0357 271.0251	Mangiferin	Xanthones	(Xu et al., 2008)
18	13.26	$C_8H_8O_5$	$[M-H]^-$	183.0299	183.0296	−1.64	168.0061 124.0159	Methyl gallate	Organic acids	(Gong et al., 2020)
19	14.36	$C_{15}H_{10}O_6$	$[M+H]^+$	287.0550	287.0554	1.39	287.0554 165.0188 153.0185 121.0289	Kaempferol	Flavonoids	(Liu et al., 2019)
*20	14.58	$C_{21}H_{20}O_{11}$	$[M-H]^-$	447.0932	447.0937	1.12	429.0831 411.0738 357.0702 369.0601 357.0623 327.0515 299.0563 285.0411	Isoorientin	Flavonoids	(Liu et al., 2019)
21	14.77	$C_{20}H_{20}O_{11}$	$[M+H]^+$	437.1078	437.1082	0.92	341.0661 317.0660 287.0555 272.0317	Irisxanthone	Xanthones	(Kim et al., 2023)
22	15.49	$C_{27}H_{30}O_{16}$	$[M-H]^-$	609.1461	609.1467	0.98	301.0358 300.0279 271.0253 151.0032	Rutin	Flavonoids	(Terpinc et al., 2016)
23	15.67	$C_{21}H_{20}O_{10}$	$[M+H]^+$	433.1129	433.1133	0.92	311.0202 283.0242	Isovitexin	Flavonoids	(Liu et al., 2019)
24	16.20	$C_{10}H_8O_4$	$[M-H]^-$	191.0350	191.0348	−1.05	176.0111 148.0160 104.0258	Scopoletin	Phenylpropanoids	(Kim et al., 2023)
25	16.38	$C_{21}H_{20}O_{12}$	$[M-H]^-$	463.0882	463.0886	0.86	343.0445 301.0357 300.0279 271.0253 255.0302 243.0298 178.9980 151.0030	Quercetin-5-O-beta-D-glucopyranoside	Flavonoids	(Liu et al., 2019)
26	16.63	$C_9H_8O_4$	$[M-H]^-$	179.0350	179.0358	4.47	135.0445 134.0365 107.0495 89.0235	Caffeic acid	Organic acids	(Liu et al., 2019)
27	17.02	$C_{25}H_{28}O_{15}$	$[M-H]^-$	567.1355	567.1352	−0.53	273.0407 258.0171 230.0219	1,5-Dihydroxy-3-methoxy-6-O-primeverosyl xanthone	Xanthones	(Wani et al., 2013)
28	17.06	$C_{11}H_{12}O_4$	$[M+H]^+$	209.0808	209.081	0.96	191.0703 163.0754 119.0494 91.0547	3,4-Dimethoxycinnamic acid	Organic acids	(Kim et al., 2023)
29	17.39	$C_{14}H_{10}O_6$	$[M+H]^+$	275.0550	275.0552	0.73	257.0447 232.0368 229.0499 201.0549	2,3,6,8-Tetrahydroxy-1-methylxanthone	Xanthones	(Kim et al., 2023)

(*continued on next page*)

Table 2 (*continued*)

No	tR/ min	Formula	Ion mode	Found at mass	Extraction mass	δ/ppm	Fragment ions	Compounds	Type	Ref
30	17.86	$C_{29}H_{30}O_{14}$	$[M-H]^-$	601.1563	601.1568	0.83	245.0459 227.0351 201.0556 141.0188	Amaroswerin	Iridoids	(Kim et al., 2023)
31	17.90	$C_{17}H_{16}O_7$	$[M+H]^+$	333.0969	333.0970	0.30	318.0736 303.0501 318.0736 285.0390 275.0550	1-Hydroxy-2,3,4,5-tetramethoxyxanthone	Xanthones	(Mou et al., 2020)
32	18.14	$C_{27}H_{30}O_{15}$	$[M-H]^-$	593.1512	593.1523	1.85	473.1093 431.0991 311.2930	Glucosylvitexin	Flavonoids	(Huang et al., 2021)
33	19.46	$C_{15}H_{10}O_6$	$[M-H]^-$	285.0405	285.0410	1.75	269.0451 253.7174 241.0512 213.0553 153.0185 135.0443 117.0341	Luteolin	Flavonoids	(Liu et al., 2019)
34	19.61	$C_{15}H_{10}O_7$	$[M-H]^-$	301.0354	301.0358	1.33	273.0045 257.0458 239.0348 107.0129	Quercetin	Flavonoids	(Liu et al., 2019)
35	20.48	$C_{14}H_{10}O_6$	$[M-H]^-$	273.0405	273.0408	1.10	258.0172 230.0221	Bellidifolin	Xanthones	(Zhang et al., 2021)
36	21.44	$C_{13}H_8O_6$	$[M-H]^-$	259.0248	259.0250	0.77	215.0348 187.0397 171.0447 159.0444	Demethylbellidifolin	Xanthones	(Swati et al., 2023)
37	22.43	$C_{13}H_8O_6$	$[M-H]^-$	259.0248	259.0250	0.77	215.0348 187.0396 171.0450 159.0442	Norswertianin	Xanthones	(Zheng et al., 2014)
38	24.86	$C_{14}H_{10}O_6$	$[M-H]^-$	273.0405	273.0407	0.73	258.0171 230.0219	Swertianin	Xanthones	(Mahendran et al., 2014)
39	25.84	$C_{14}H_{10}O_6$	$[M-H]^-$	273.0405	273.0407	0.73	258.0171 230.0220	Isobellidifolin	Xanthones	(Swati et al., 2023)
40	27.28	$C_{17}H_{16}O_7$	$[M+H]^+$	333.0969	333.0971	0.60	318.0736 303.0501 318.0736 285.0390 275.0551	1-Hydroxy-2,3,4,7-tetramethoxyxanthone	Xanthones	(Mou et al., 2020)
41	27.92	$C_{16}H_{14}O_6$	$[M+H]^+$	303.0863	303.0864	0.33	288.0630 273.0395 270.0524 259.0604 245.0446	8-Hydroxy-1,3,5-trimethoxyxanthone	Xanthones	(Jia et al., 2011)
42	28.66	$C_{15}H_{12}O_5$	$[M+H]^+$	273.0758	273.0758	0.00	258.0525	1-Hydroxy-3,5-dimethoxyxanthone	Xanthones	(Swati et al., 2023)
43	29.45	$C_{15}H_{12}O_6$	$[M+H]^+$	289.0707	289.0709	0.69	274.0474 256.0367 246.0525	1,8-Dihydroxy-3,5-dimethoxyxanthone	Xanthones	(Swati et al., 2023)
44	29.76	$C_{15}H_{12}O_6$	$[M+H]^+$	289.0707	289.0709	0.69	274.0474 256.0367 246.0492 228.0420	1,8-Dihydroxy-3,7-dimethoxyxanthone	Xanthones	(Swati et al., 2023)
45	31.49	$C_{30}H_{46}O_4$	$[M+H]^+$	471.3469	471.3474	1.06	453.3367 189.1641	Glycyrrhetinic acid	Organic acids	(Zheng et al., 2022)
46	34.56	$C_{30}H_{48}O_4$	$[M+H]^+$	473.3625	473.3633	1.69	427.3678 409.3469 255.2125 207.1747 203.1796 201.1641 189.1639 135.1170 121.1017 107.0860	Maslinic acid	Terpenes	(Kim et al., 2023)
47	37.73	$C_{30}H_{48}O_3$	$[M+H]^+$	457.3676	457.3682	1.31	439.3578 411.3625 393.3507 249.1844 191.1795	Oleanolic acid	Terpenes	(Chen et al., 2011)
*48	38.22	$C_{30}H_{48}O_3$	$[M+H]^+$	457.3676	457.3697	4.59	439.3596 411.3626 393.3474 249.1849 191.1794	Ursolic Acid	Terpenes	(Wang et al., 2016)
49	38.98	$C_{18}H_{30}O_2$	$[M+H]^+$	279.2319	279.2331	4.30	261.2215 243.2114 223.1699 137.1327 123.1172 109.1017 95.0862 81.0706	Linolenic acid	Fatty acids	(Kapoor and Huang 2006)

* standard substances.

3.1.1. *Mangiferin*

The compound under investigation, known as Mangiferin, exhibited a retention time of 12.71 min. Its molecular formula is $C_{19}H_{18}O_{11}$, and the mass spectral signal for its quasi-molecular ion peaks $[M-H]^-$ was detected at *m/z* 421.0782, with a negligible error of 1.42 ppm. The compound's secondary mass spectra revealed characteristic fragment ions at *m/z* 331.0463, *m/z* 301.0357, and *m/z* 271.0251. Notably, the ions observed at *m/z* 331.0471 and *m/z* 301.0375 correspond to $[M-H-C_3H_6O_3]^-$ and $[M-H-C_4H_8O_4]^-$ mass spectrometric fragments, respectively, resulting from internal sugar breakage. These findings, along with a reference to previous work (Xu et al., 2008), confirm the identification of the compound as Mangiferin. The cleavage pattern of Mangiferin is depicted in Fig. 3A.

3.1.2. *1-Hydroxy-2,3,4,5-tetramethoxyxanthone*

The compound of interest exhibited a retention time of 17.9 min. Its molecular formula was determined as $C_{17}H_{16}O_7$ and the mass spectral signal of its quasi-molecular ion peaks $[M+H]^+$ was recorded at *m/z* 333.0970, with a deviation of 0.30 ppm. The secondary mass spectra displayed characteristic fragment ions at *m/z* 318.0736, *m/z* 303.0501, *m/z* 318.0736, *m/z* 285.0390, and *m/z* 275.0550. The ion *m/z* 318.0739 represents the fragment $[M+H\text{-}CH_3]$, which is formed by the removal of one methyl molecule from the precursor ion $[M+H]^+$. Meanwhile, *m/z* 303.0515 corresponds to the fragment $[M+H]^+$ formed by the simultaneous loss of two methyl group molecules $[M+H\text{-}2CH_3]^+$. Further, fragments at *m/z* 285.0385 and 275.0589 are likely the ions $[M+H\text{-}2CH_3\text{-}H_2O]^+$ and $[M+H\text{-}2CH_3\text{-}CO]^+$, respectively, resulting from neutral losses of H_2O (18 Da) and CO (28 Da) at *m/z* 303.0515. Hence, based on this analysis, the compound has been identified as 1-Hydroxy-2,3,4,5-tetramethoxyxanthone (Mou et al., 2020). The cleavage pattern of 1-Hydroxy-2,3,4,5-tetramethoxyxanthone is presented in Fig. 3B.

3.1.3. *Caffeic acid*

The compound under analysis had a retention time of 16.63 min. Its

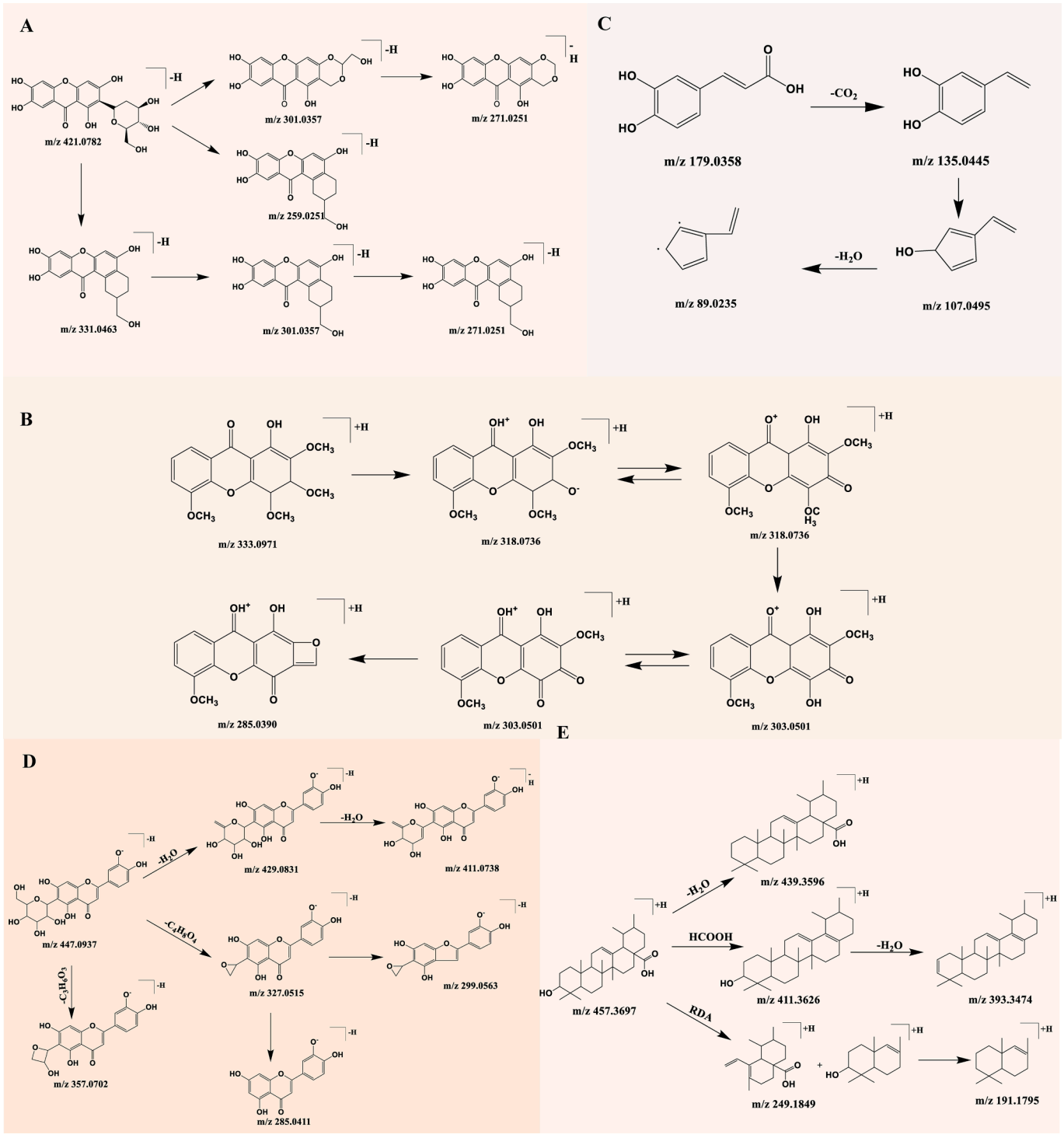

Fig. 3. Diagram of cleavage pattern of chemical composition of 80% ethanolic extract of *S. chirayita*.

molecular formula was determined as $C_9H_8O_4$ and the mass spectral signal of its quasi-molecular ion peaks $[M-H]^-$ was recorded at *m/z* 179.0358, with a deviation of 4.47 ppm. The secondary mass spectra exhibited characteristic fragment ions at *m/z* 135.0445, *m/z* 107.0495, and *m/z* 89.0235. Based on these findings and referencing to previous work (Xiao et al., 2022), the compound was identified as caffeic acid. The cleavage pattern of caffeic acid is illustrated in Fig. 3C.

3.1.4. *Isoorientin*

The compound of interest exhibited a retention time of 14.58 min and was identified as $C_{21}H_{20}O_{11}$ based on the inferred molecular formula. Mass spectral analysis showed a quasi-molecular ion peak $[M-H]^-$ at *m/z* 447.0937, with a minimal error of 1.12 ppm. The secondary mass spectra of the compound displayed characteristic fragment ions at *m/z* 429.0831, *m/z* 411.0738, *m/z* 357.0702, *m/z* 327.0515, *m/z* 299.0563, and *m/z* 285.0411. Notably, the ions observed at *m/z* 357.0617 and *m/z* 327.0514 could indicate neutral losses of 90 Da and 120 Da, respectively, which are common features in C-glycosides. These findings, along with support from existing literature (Liu et al., 2019), confirm the identification of the compound as isoorientin. The fragmentation

pathway of isoorientin is depicted in Fig. 3D.

3.1.5. Ursolic acid

The compound exhibited a retention time of 37.73 min. Its molecular formula was determined to be $C_{30}H_{48}O$, and the mass spectral signal showed quasi-molecular ion peaks $[M+H]^+$ at *m/z* 457.3697, with a minimal error of 4.59 ppm. Secondary mass spectra exhibited characteristic fragment ions at *m/z* 439.3596, *m/z* 411.3626, *m/z* 249.1849, and *m/z* 191.1795. The losses of neutral molecules H_2O (18 Da) and HCOOH (46 Da), as well as the *retro*-Diels-Alder (RDA) fragmentation of the C ring, were identified based on previous literature (Wang et al., 2015). Therefore, this compound can be identified as ursolic acid. The fragmentation pattern is illustrated in Fig. 3E.

3.2. Analysis of serum pharmacochemistry of S. chirayita

Due to the complex chemical composition of TCM/ethnomedicines, it is more effective to analyze the process of how they enter the body and identify their blood-entry components when applying network pharmacology to the study of TCM/ethnomedicines. Blood-entry components are considered as potential bioactive components of TCM/ethnomedicines that exert pharmacological effects. Therefore, an examination of the blood entry prototype components of *S. chirayita* in rats was conducted using the UPLC-Q-Exactive Orbitrap MS technique. As a result, a total of 10 blood-entry prototype components was successfully identified, including swertianlarin, sweroside, mangiferin, bellidifolin, and isobellidifolin, among others (Figs. 4, 5, and Table 3). In conclusion, these findings confirm that these ten blood-entry prototype components may be the main components of *S. chirayita* responsible for its medicinal effects.

3.3. Network pharmacology analysis

3.3.1. Potential targets prediction

To clarify the potential targets of *S. chirayita* against ALI, we used the SwissTargetPrediction database to predict the potential targets of 10 blood-entry prototype components of *S. chirayita*. And 310 relevant targets were obtained. Additionally, 1,803 ALI-associated targets we identified based on GeneCards and OMIM databases. By using the Venny online tool, 148 potential common targets were obtained (Fig. 6A). These 148 targets are considered as potential targets for *S. chirayita* to exert its anti-ALI effects.

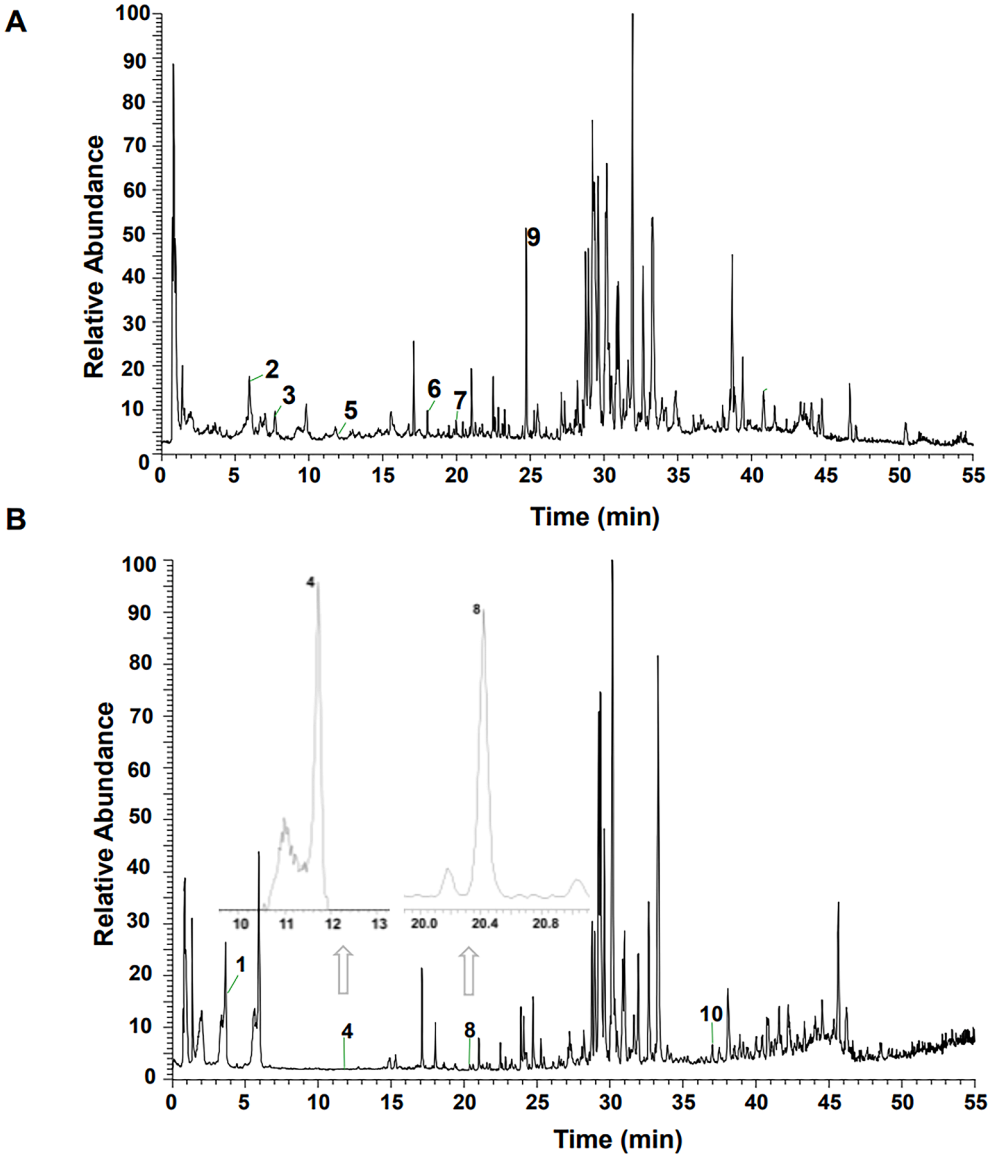

Fig. 4. TIC of drug-containing plasma in the negative (A) and positive (B) ion modes.

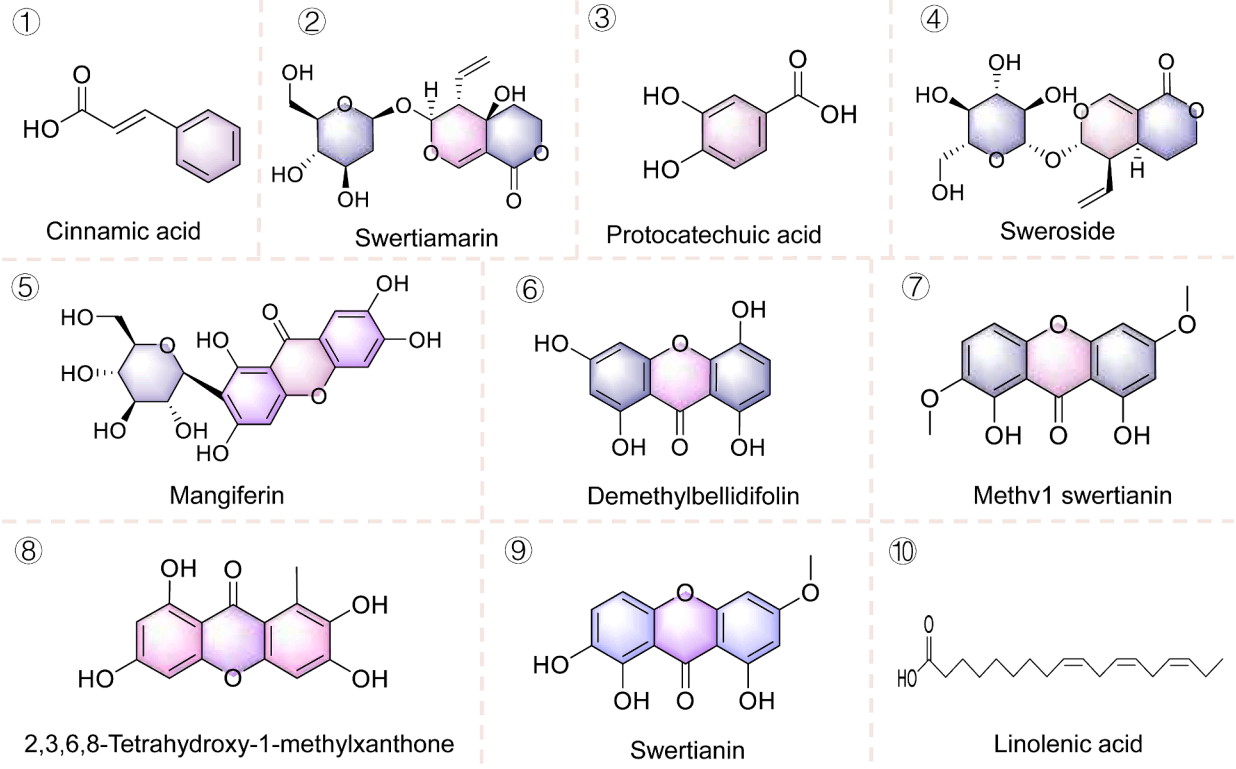

Fig. 5. The structure of prototypic components of 80 % ethanolic extract of *S. chirayita* in the serum of SD rats.

Table 3
Identification chemical components of 80 % ethanolic extract of *Swertia chirayita* absorbed in the blood using UPLC-Q-Exactive Orbitrap MS.

No	tR/ min	Formula	Ion mode	Found at mass	Extraction mass	δ/ppm	Fragment ions	Compounds	Type
1	3.62	$C_9H_8O_2$	$[M+H]^+$	149.0597	149.0601	2.68	131.0495 121.0652 107.0497 79.0549	Cinnamic acid	Organic acids
2	6.19	$C_{16}H_{22}O_{10}$	$[M-H]^-$	373.1140	373.1143	0.80	193.0352 149.5000 113.0237 89.0234 85.0286 71.0129 59.0128	Swertiamarin	Iridoids
3	7.18	$C_7H_6O_4$	$[M-H]^-$	153.0193	153.0188	−3.28	125.0236 109.0288 108.0210	Protocatechuic acid	Organic acids
4	11.72	$C_{16}H_{22}O_9$	$[M+H]^+$	359.1337	359.1346	2.51	197.0815 154.9906 110.0207	Sweroside	Iridoids
5	12.57	$C_{19}H_{18}O_{11}$	$[M-H]^-$	421.0776	421.0784	1.90	331.0464 301.0358 271.0258 259.0245	Mangifera	Xanthones
6	18.75	$C_{13}H_8O_6$	$[M-H]^-$	259.0248	259.0251	1.16	215.0343 187.0394	Demethylbellidifolin	Xanthones
7	19.95	$C_{13}H_8O_6$	$[M-H]^-$	259.0248	259.0252	1.54	215.0352 187.0395	Methv1swertianin	Xanthones
8	20.42	$C_{14}H_{10}O_6$	$[M+H]^+$	275.055	275.0554	1.45	232.0371 229.0503 201.0551	2,3,6,8-Tetrahydroxy-1-methylxanthone	Xanthones
9	24.57	$C_{14}H_{10}O_6$	$[M-H]^-$	273.0405	273.041	1.83	258.0173 230.0221	Swertianin	Xanthones
10	36.53	$C_{18}H_{30}O_2$	$[M+H]^+$	279.2319	279.2326	2.51	261.2224 243.2121 223.1703 149.0237 137.1328 123.1173 109.1018 95.0862 81.0707	Linolenic acid	Others

3.3.2. *PPI network analysis and enrichment analysis*

To investigate the potential function and mechanism of action of *S. chirayita* on ALI, we conducted PPI network analysis and enrichment analysis on the 148 cross-targets mentioned earlier. Firstly, the STRING database was utilized to construct a PPI network comprising these 148 common targets (Fig. 6B). This network was crucial in understanding how *S. chirayita* intervenes in ALI, as all of these genes were included. Subsequently, the cytoHubba plug-in in Cytoscape 3.7.1 were employed to filter the top targets based on their degree value, resulting in the identification of the top 10 targets, which included EGFR, CASP3, CTNNB1, STAT3, SRC, ESR1, PTGS2, PPARG, TLR4 and MMP9 (Fig. 6C). Taken together, these 10 targets were deemed as the core targets responsible for *S. chirayita*'s anti-ALI effects. GO analysis revealed that these ten typical blood components could potentially regulate ALI through biological processes such as drug response and positive regulation of apoptosis (Fig. 6D). Furthermore, KEGG analysis suggested that S. chirayita might govern ALI through various signaling pathways, including the PI3K/Akt pathway, HIF-1 pathway, MAPK pathway, VEGF pathway, AMPK signaling pathway, FoxO signaling pathway, JAK/STAT signaling pathway, NF-κB signaling pathway, among others (Fig. 6E and Table 4).

3.4. *Molecular docking analysis*

Molecular docking simulations were used to investigate the interaction dynamics between the ten blood-entry prototype components of *S. chirayita* and key protein targets associated with ALI. The top ten targets, including EGFR, CASP3, CTNNB1, STAT3, SRC, ESR1, PTGS2, PPARG, TLR4, and MMP9 (Fig. 6C and Table 5). These targets exhibited strong binding potential with *S. chirayita* constituents, as indicated by

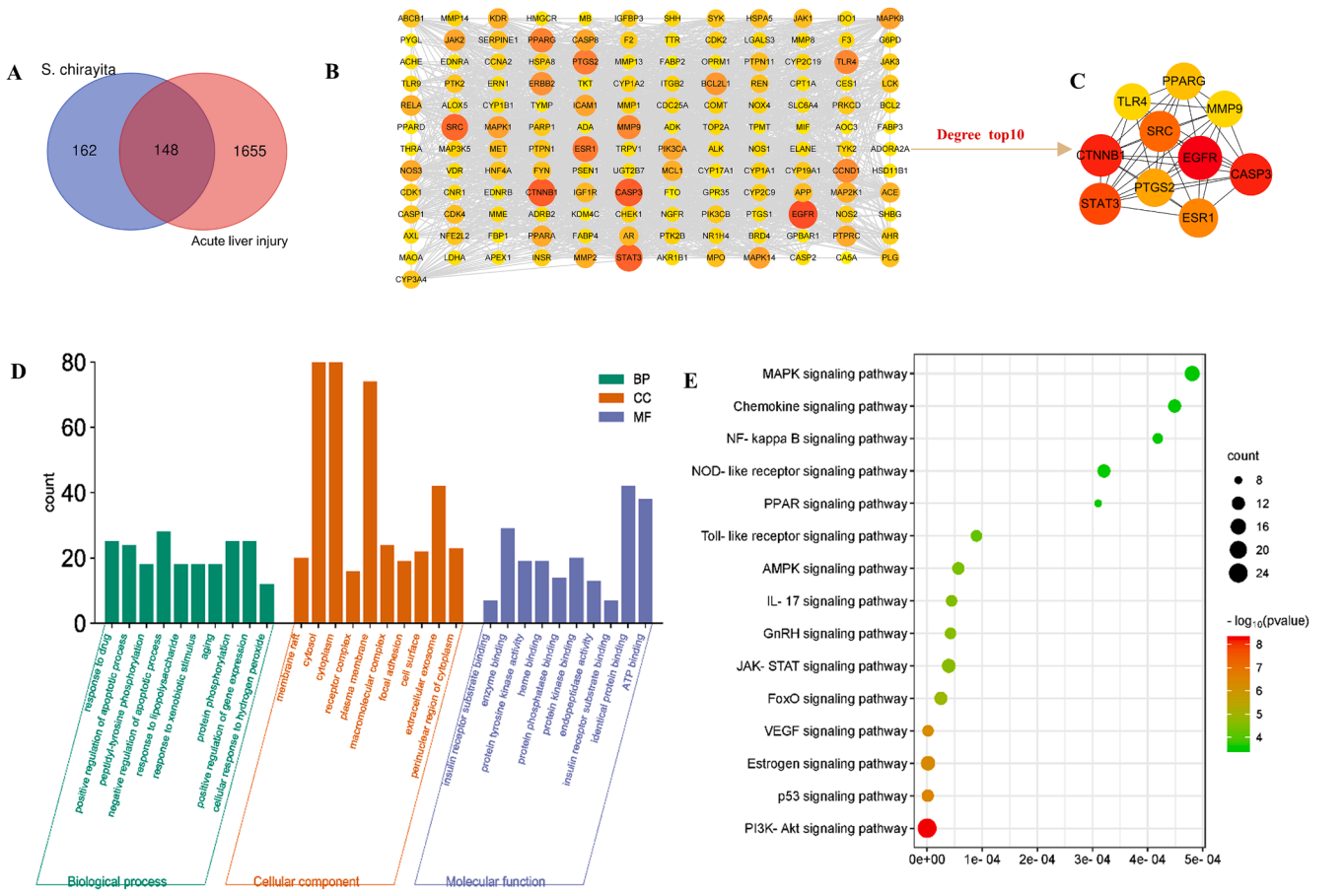

Fig. 6. Hub genes of the chemical components of 80 % ethanolic extract of *S. chirayita* absorbed in blood and acute liver injury. (A) Venn diagram and candidate targets of the chemical components of 80 % ethanolic extract of *S. chirayita* absorbed in blood and acute liver injury, (B) Protein-protein interaction (PPI) network, (C) KEGG enrichment diagram, (D) GO including CC, MF, and BP analysis diagram, (E) Molecular docking heat map of 10 core targets with 10 critical compounds. The color represents the binding ability. The greener the color, the lower the binding ability and the higher the affinity between the receptor and the ligand.

Table 4
The analysis of KEGG enrichment of *Swertia chirayita* and ALI.

No	Signaling pathway	FDR	PValue	Count
1	HIF-1 signaling pathway	3.85E-10	3.01E-11	17
2	PI3K-Akt signaling pathway	2.72E-08	4.5E-09	25
3	p53 signaling pathway	1.23E-06	3.52E-07	11
4	Estrogen signaling pathway	1.71E-06	5.22E-07	14
5	VEGF signaling pathway	1.73E-06	5.43E-07	10
6	FoxO signaling pathway	2.51E-05	1.24E-05	12
7	JAK-STAT signaling pathway	3.93E-05	2.28E-05	13
8	GnRH signaling pathway	4.26E-05	2.55E-05	10
9	IL-17 signaling pathway	4.45E-05	2.78E-05	10
10	AMPK signaling pathway	5.67E-05	3.6E-05	11
11	Toll-like receptor signaling pathway	8.96E-05	6.23E-05	10
12	PPAR signaling pathway	0.00031	0.000262	8
13	NOD-like receptor signaling pathway	0.000321	0.000276	12
14	NF-kappa B signaling pathway	0.000418	0.000364	9
15	Chemokine signaling pathway	0.000449	0.000398	12
16	MAPK signaling pathway	0.000481	0.000439	15
17	Adipocytokine signaling pathway	0.001118	0.001059	7

Table 5
The degree value of top 10 targets of *Swertia chirayita* and ALI.

No	Targets	Name of targets	Uniprot ID	Degree
1	EGFR	Epidermal growth factor receptor	P00533	86.0
2	CASP3	Caspase-3	P42574	80.0
3	CTNNB1	Catenin beta-1	P35222	80.0
4	STAT3	Signal transducer and activator of transcription 3	P40763	78.0
5	SRC	Proto-oncogene tyrosine-protein kinase Src	P12931	75.0
6	ESR1	Estrogen receptor	P03372	69.0
7	PTGS2	Prostaglandin G/H synthase 2	P35354	66.0
8	PPARG	Peroxisome proliferator-activated receptor gamma	P37231	63.0
9	TLR4	Toll-like receptor 4	O00206	61.0
10	MMP9	Matrix metalloproteinase-9	P14780	61.0

docking scores surpassing the threshold of −6 (Fig. 7 and Table 6). These findings suggest that the constituents of *S. chirayita*, particularly STW, may play a significant role in the herb's therapeutic efficacy in ALI.

3.5. Network analysis of STW in ALI

Swertiamarin has been traditionally used in the treatment of liver diseases and has shown promising hepatoprotective effects in preliminary studies. Based on the results of blood component analysis and molecular docking, STW was hypothesized is the crucial chemical component for *S. chirayita* in its anti-ALI effects. All in all, this historical and preliminary evidence provided a strong foundation for its selection as a focus for our detailed investigation. To further investigate, a network of potential targets involved in the anti-ALI properties of STW was constructed. The result revealed a total of 139 targets associated with the anti-ALI effects of STW (Supplementary Fig. S3A). Among these targets, EGFR, CASP3, CTNNB1, STAT3, ESR1, PTGS2, PPARG, TLR4, and MMP9 were identified as key targets in the anti-ALI intervention of

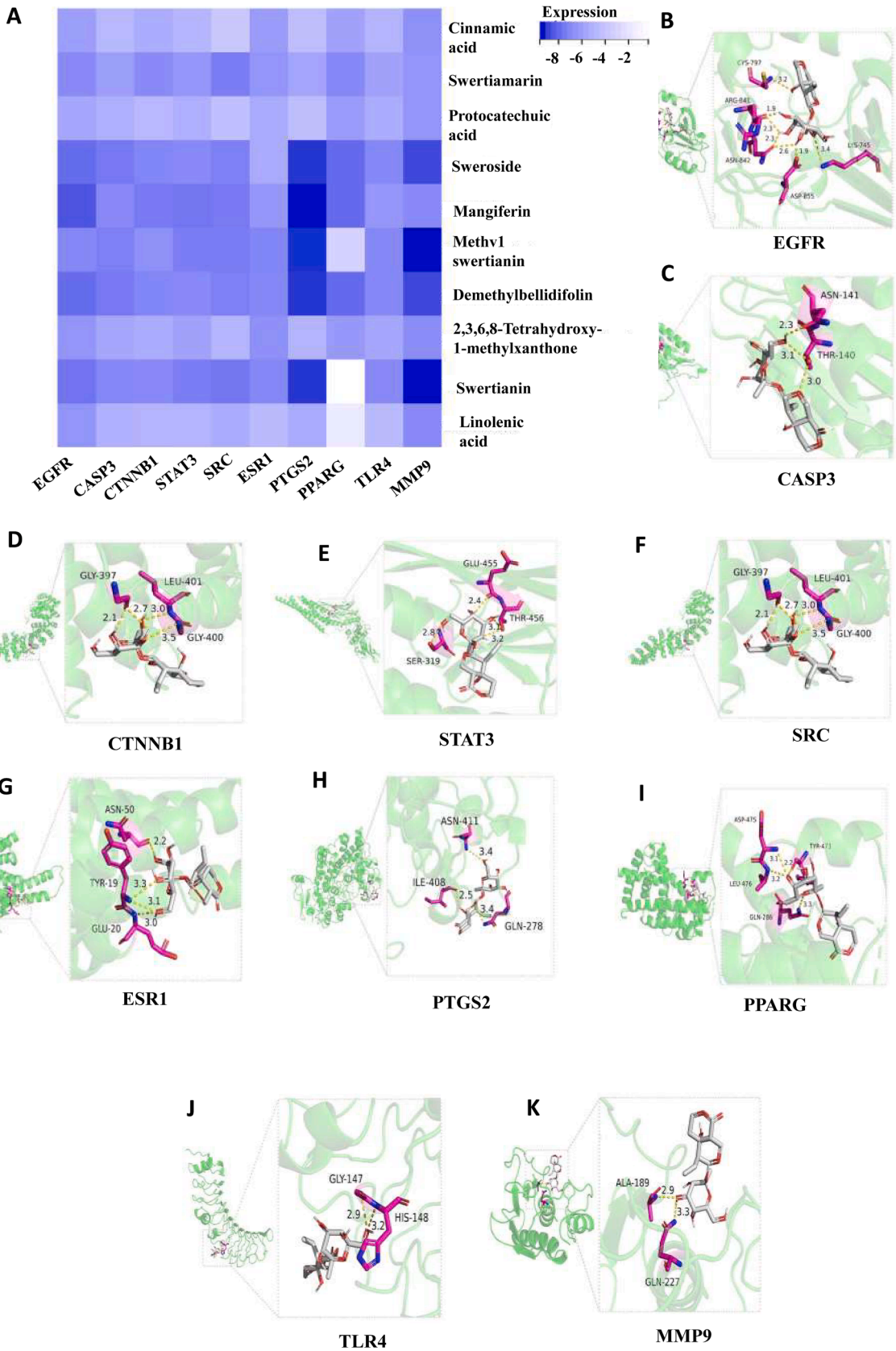

Fig. 7. Docking patterns of 10 targets with STW with the lower binding ability. (A) EGFR&STW, (B) CASP3&STW, (C) CTNNB1&STW, (D) STAT3&STW, (E) SRC&STW, (F) ESR1&STW, (G) PTGS2&STW, (H) PPARG&STW, (I) TLR4&STW, (J) MMP9&STW.

Table 6
The binding ability of 10 prototypical blood components and 10 core targets docking junction.

Compounds	EGFR 3w2s	CASP3 1nme	CTNNB1 6 m90	STAT3 6njs	SRC 3vro	ESR1 7baa	PTGS2 5f1a	PPARG 3sz1	TLR4 3ul7	MMP9 6esm
Cinnamic acid	−6.3	−5	−5.6	−5.1	−4	−6.4	−4.7	−6.1	−5.2	−6.9
Swertianmarin	−7.1	−6.3	−7.1	−6.6	−7.6	−6.7	−6	−7.2	−6.1	−6.7
Protocatechuic acid	−5.9	−5.5	−5	−5.5	−4.5	−5.7	−4.7	−6.4	−5.6	−6.7
Sweroside	−8.1	−7.7	−7.3	−7.1	−7.5	−5.7	−9.3	−8.2	−7.2	−9.0
Mangiferin	−8.7	−7.1	−7.7	−7.8	−7.7	−6.6	−9.6	−8.2	−6.6	−7.1
Methv1swertianin	−7.2	−7.5	−6.9	−7.6	−7.6	−7.3	−9.4	−3.3	−7.2	−9.6
Demethylbellidifolin	−8.1	−7.7	−7.3	−7.1	−7.5	−7.2	−9.3	−8.2	−7.2	−9.0
2,3,6,8-Tetrahydroxy-1-methylxanthone	−6.7	−5.9	−5.6	−6.1	−5.1	−6.9	−5.2	−6.5	−5.9	−7.0
Swertianin	−7.9	−7.2	−7.1	−7.6	−7.8	−7.2	−9.3	−0.3	−7.1	−9.6
Linolenic acid	−6.7	−5.4	−5.2	−5.3	−5.6	−4.9	−5.7	−1.8	−4.9	−7.1

S. chirayita (Supplementary Fig. S3B). Notably, CTNNB1, STAT3, ESR1, PTGS2, PPARG, TLR4, and MMP9 were also found to be key targets in the ALI intervention of STW. This finding further supports our molecular docking results. In summary, STW was conclude that is the key pharmacodynamic substance responsible for the anti-ALI effects of *S. chirayita*. Therefore, the anti-ALI pharmacodynamic effects of STW was subsequently verified.

3.6. Analysis of the intervention of the STW in CCl_4-induced ALI

3.6.1. Analysis of liver index

An evaluation of the liver index following STW administration offers insights into the therapeutic impact of *S. chirayita* on liver pathology. In mouse models subjected to CCl_4-induced hepatic injury, treatment with STW significantly decreased the liver index, serving as an indicator of reduced organ swelling and damage. Compared to the blank group,

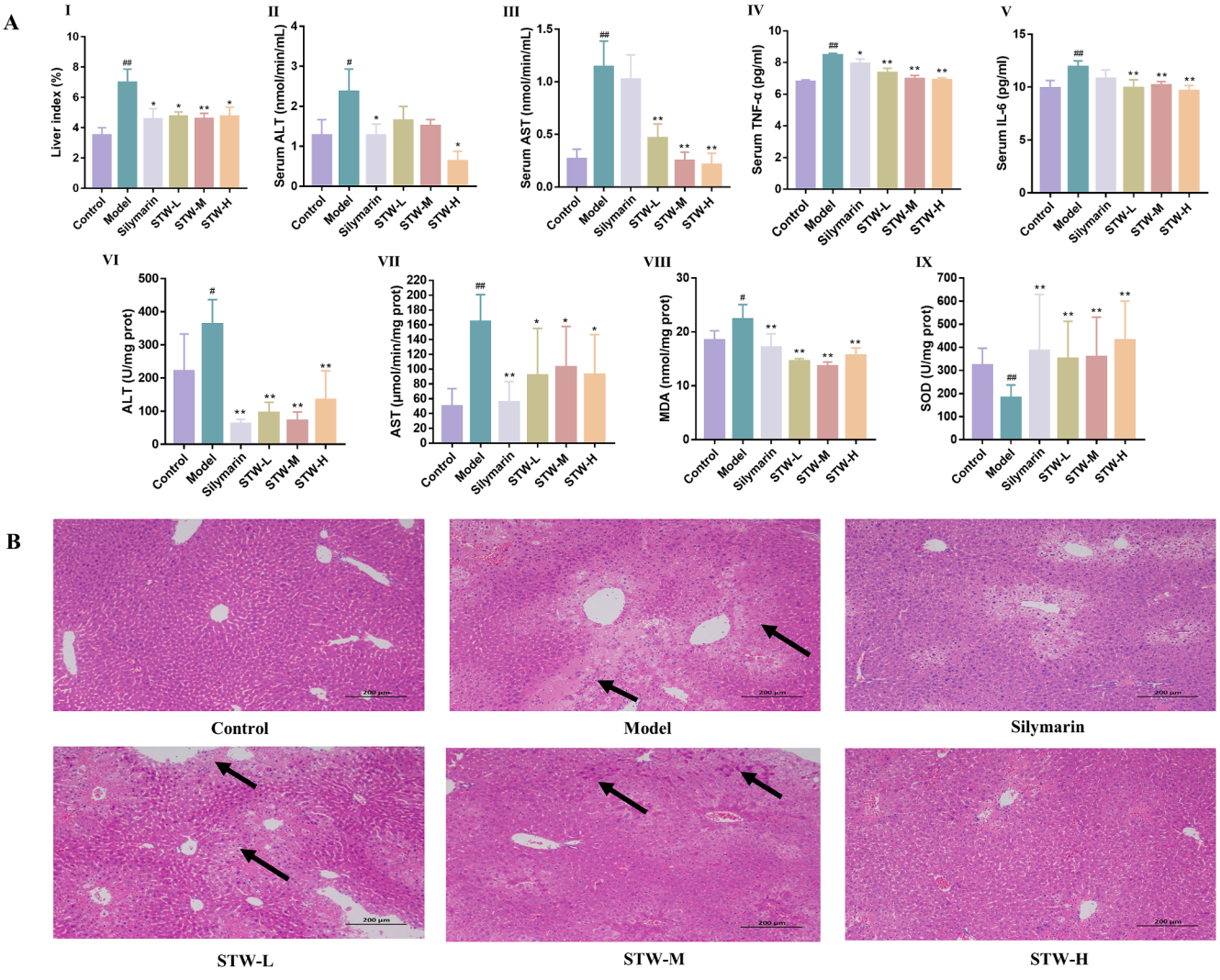

Fig. 8. (A) Effect of the liver index, the biochemistry of serum and liver tissue in CCl_4-induced acute liver injury model. (I) liver index, (II) concentration of ALT in serum, (III) concentration of AST in serum, (IV) concentration of TNF-α in serum, (V) concentration of IL-6 in serum, (VI) concentration of ALT in liver, (VII) concentration of AST in liver, (VIII) concentration of MDA in liver, (IX) concentration of SOD in liver. (B) STW ameliorates induced histopathological changes in the liver tissues of CCl_4-induced acute liver injury model. $^{\#}p < 0.05$, $^{\#\#}p < 0.01$, vs. the control group; $^{*}p < 0.05$, $^{**}p < 0.01$, vs. the model group.

those in the model group exhibited a statistically significant increase in liver index ($p < 0.01$). In contrast, administration of STW at varying doses, as well as silymarin, distinctly attenuated the liver index, suggesting a dose-responsive protective effect against the hepatic injury ($p < 0.05$) (Fig. 8A). These findings underscore the potential of STW as a mitigating agent in CCl_4-induced liver damage.

3.6.2. Biochemical analysis of the serum

When exposed to high quantities of CCl_4, the liver is attacked, resulting in an excessive production of free radicals. This, in turn, increases the permeability of cell membranes, leading to the infiltration of inflammatory neutrophils and a significant influx of ALT, AST, TNF-α, and IL-6 into the bloodstream. These factors contribute to the elevated serum levels (Masuda 2006, Niu et al., 2017). Our findings demonstrate a statistically significant reduction in ALT levels among subjects treated with silymarin or STW-H groups compared to the model group, indicating a protective effect on the liver ($p < 0.05$). Similarly, AST, TNF-α, and IL-6 levels were significantly lower in all STW dosed groups (low, medium, and high), as well as the silymarin-treated group, in comparison to the model group. This highlights the potential of the treatment to alleviate the inflammatory response associated with hepatic injury (Fig. 8A). These differences emphasize the therapeutic potential of STW in mitigating CCl_4-induced hepatic damage.

3.6.3. Biochemical analysis of the liver

The therapeutic efficacy of STW in acute CCl_4-induced hepatic injury was evaluated by examining liver biochemical parameters. Since the liver is the primary site of acute CCl_4-induced ALI (Dong et al., 2013), it was important to assess the effects of STW. Compared to the control group, all STW treatment protocols (low, medium, and high doses) as well as silymarin administration showed significant improvements in hepatic ALT, AST, MDA, and SOD levels ($p < 0.01$). These findings not only support the serum biochemical results but also provide additional evidence that STW has a hepatoprotective effect against CCl_4-induced damage. This reinforces the potential use of STW for intervention in CCl_4-induced ALI (Fig. 8A).

3.6.4. Histological analysis of the liver

Histopathological examinations were conducted using H&E staining to provide a detailed understanding of the hepatoprotective impact of STW. In the control group, liver sections exhibited well-preserved lobular architecture, orderly arranged hepatocytes, and intact liver capsule structures without any swelling or inflammatory infiltration. In contrast, liver samples from the CCl_4-induced model group showed extensive inflammatory infiltrate surrounding vascular structures, along with significant hepatocellular degeneration and necrosis. Treatment with different dosages of STW (low, medium, and high) and silymarin resulted in significant improvements in these pathological changes. The extent of improvement in inflammatory infiltration, edema, degeneration, and necrosis of hepatocytes varied depending on the treatment concentration, but was observed in all treated groups (Fig. 8B). Notably, the group receiving the highest dosage of STW (STW-H) exhibited the most substantial amelioration of CCl_4-induced liver damage, highlighting the potential of STW in counteracting hepatic insult.

3.6.5. Analysis of qRT-PCR

To substantiate the interactions proposed by our network pharmacology framework, we used qRT-PCR to evaluate the gene expression of pivotal targets. The results showed that STW administration significantly downregulated the mRNA levels of EGFR (Fig. 9A), CASP3 (Fig. 9B), CTNNB1 (Fig. 9C), STAT3 (Fig. 9D), ESR1 (Fig. 9F), PTGS2 (Fig. 9G), PPARG (Fig. 9H), TLR4 (Fig. 9I) and MMP9 (Fig. 9J). Interestingly, SRC expression was found to be upregulated upon STW treatment (Fig. 9E). These expression patterns not only confirmed the network pharmacology predictions but also validated the target-related pathways involved in the therapeutic action of STW. The alignment of these qRT-PCR findings with the in-silico data provides strong evidence for the regulatory role of STW on these key genetic targets, strengthening the credibility of the computational strategies used to understand the molecular basis of *S. chirayita*'s pharmacological effects.

3.6.6. Analysis of molecular dynamics and immunohistochemistry

To enhance the validation of molecular docking individual qRT-PCR results, we combined both expression levels and selected the target with an expression level greater than 15 and a molecular docking score lower than -6.5 kcal·mol^{-1} for further validation. The molecular dynamics findings indicated that STW effectively bound to both ESR1 and MMP9. Specifically, the RSMD analysis revealed that the RMSD curves of ESR1 and MMP9 proteins in complex with STW stabilized after initial fluctuations, with fluctuations remaining within 0.5 nm, indicating a stable binding formation between them and STW (Fig. 9K). The RMSF curves for ESR1 and MMP9 proteins in complex with STW did not fluctuate beyond 1 nm, with no amino acid residues showing significant fluctuations, suggesting that STW did not affect the overall structural stability of the proteins (Fig. 9L). Rg (Fig. 9M) and SASA (Fig. 9N) results confirmed that the addition of STW did not notably impact the overall structural stability of the protein. The free energy landscape map displayed a single minimum energy cluster for both ESR1 and MMP9 in association with STW, indicating a high stability of the complex formed by them with STW (Fig. 9O). The results from the analysis of hydrogen bond quantity revealed that ESR1, MMP9, and STW all formed stable hydrogen bonding interactions (Fig. 9P). Additionally, to further elucidate the protein levels of ESR1 and MMP9, an immunohistochemistry assay was conducted. The findings demonstrated that STW notably enhanced the protein expression levels of ESR1 and MMP9 (Fig. 9Q), providing further evidence that these targets could be crucial for the intervention of swertiamarin in acute liver injury. The consistency between the results of immunohistochemistry, molecular dynamics, and PCR underscored the promising potential of bioinformatics analysis in drug research.

4. Discussion

Our integrative analysis of *S. chirayita* through UPLC-Q-Exactive Orbitrap MS has successfully demystified the plant's pharmacologically active constituents, identifying 49 chemical entities with potential medicinal relevance. These entities span a diverse array of phytochemical classes, including xanthones, organic acids, flavonoids, and terpenoids, which may collectively contribute to the observed medicinal properties of the herb. Intriguingly, these chemical investigations align with traditional claims of S. chirayita's therapeutic versatility and offer a foundation for understanding the molecular basis of its efficacy. Furthermore, the precise fragmentation patterns elucidated for compounds like mangiferin and 1-Hydroxy-2,3,4,5-tetramethoxyxanthone enable accurate identification and deepen our understanding of their intrinsic pharmacodynamic profiles.

Pharmacokinetic studies have demonstrated that the absorption of a drug is the primary stage in the therapeutic mechanism of a medication (Lin et al., 2022). Presently, oral administration is the most common route for traditional Chinese medicines, with their active constituents primarily transported to target sites through the bloodstream to achieve an optimal blood concentration (Tan et al., 2023). The components present in the blood are deemed vital for eliciting therapeutic effects. Consequently, extending beyond compound characterization, our serum pharmacochemical analysis pinpointed ten blood-entry components, including STW, sweroside, and others, that may play a cardinal role in mediating *S. chirayita*'s therapeutic effects *in vivo*. This vital insight bridges the traditional usage of the herb with a contemporary understanding of its bioactive constituents.

The network pharmacology approach further refined our exploration using the ten blood-entry components, pinpointing potential molecular targets and signaling pathways that *S. chirayita* might modulate. Key

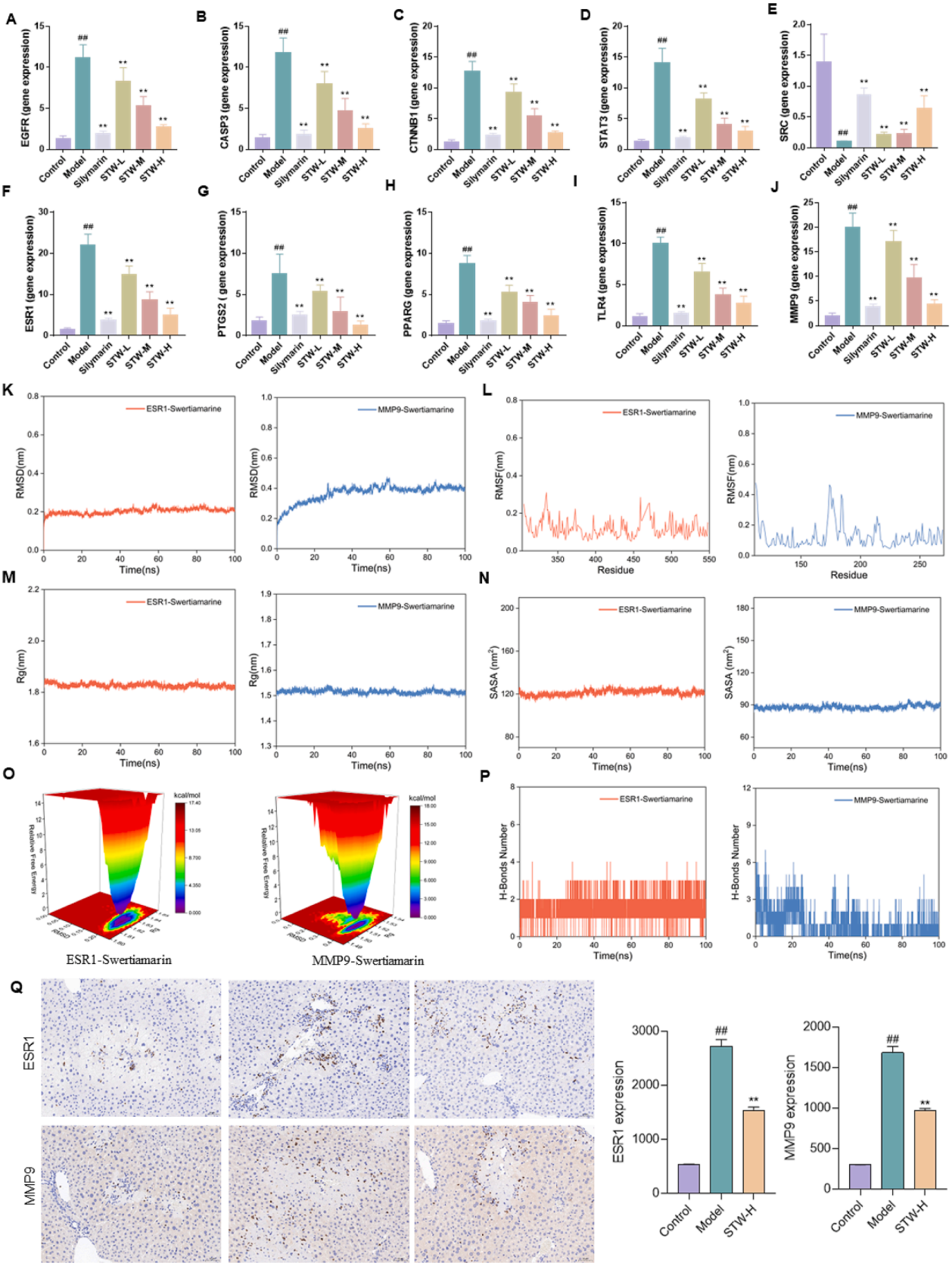

Fig. 9. Potential targets for STW intervention in a CCl_4-induced acute liver injury model. (A) mRNA level of EGFR, (B) mRNA level of CASP3, (C) mRNA level of CTNNB1, (D) mRNA level of STAT3, (E) mRNA level of SRC, (F) mRNA level of ESR1, (G) mRNA level of PTGS2, (H) mRNA level of PPARG, (I) mRNA level of TLR4, (J) mRNA level of MMP9. (K) RMSD analysis of ESR1 and MMP9 with STW, (L) RMSF analysis of ESR1 and MMP9 with STW, (M) Rg analysis of ESR1 and MMP9 with STW, (N) SARA analysis of ESR1 and MMP9 with STW, (O) Free energy landscape map analysis of ESR1 and MMP9 with STW, (P) H-Bounds number analysis of ESR1 and MMP9 with STW, (Q) IHC analysis of ESR1 and MMP9 in liver. $^{\#}p < 0.05$, $^{\#\#}p < 0.01$, vs. the control group; $^{*}p < 0.05$, $^{**}p < 0.01$, vs. the model group.

amongst these, EGFR, CASP3, and STAT3 were identified as central nodes within a complex therapeutic network, potentially orchestrating the plant's protective effects against ALI. The KEGG analysis revealed that *S. chirayita* may impact ALI through various signaling pathways, such as PI3K/Akt, HIF-1, MAPK, FoxO, JAK/STAT, and NF-κB, among others. Previous studies have suggested that oxidative stress and inflammation play a role in the pathogenesis and progression of CCl_4-induced ALI (Zhan et al., 2021, Bekkouch et al., 2022). The NF-κB signaling pathway is well-known for its association with inflammation. Previous studies have shown that cyanidin effectively reduces the symptoms of CCl_4-induced ALI by suppressing targets related to the NF-κB signaling pathway (Wang et al., 2022a,b). Similarly, evidence suggests that the JianPi-QingHua formula significantly improves the dysregulation of inflammatory factors in a nonalcoholic steatohepatitis model by modulating critical elements within the NF-κB pathway, thereby providing hepatoprotective effects (Tian et al., 2023). The PI3K/AKT signaling pathway acts as a negative feedback mechanism for Toll-like receptor signaling, limiting the pro-inflammatory response in LPS-stimulated macrophages and promoting an anti-inflammatory response by regulating the expression of miRNAs for TLR4 and SOCS111 (Liu et al., 2023). Another study reveals that fraxin exerts hepatoprotective effects by inhibiting MAPK and NF-κB activation. This is achieved by reducing the expression of MAPKs, NF-κB, and COX-2 proteins in the liver tissue of mice with CCl_4-induced liver injury (Niu et al., 2017). The HIF-1 is a heterodimer composed of both HIF1-α and HIF1-β subunits. Under hypoxic conditions, HIF1-α upregulates the expression of p53 protein, leading to its accumulation. In the same conditions, p53 can directly interact with HIF1-α to prevent the expression of HIF1-α induced by hypoxia. This interaction promotes MDM2-mediated ubiquitination and proteasomal degradation (Chu et al., 2022). Previous studies have shown the involvement of HIF-1 in various liver diseases, including acetaminophen (APAP)-induced liver injury, fatty liver, alcoholic hepatitis, nonalcoholic steatohepatitis (Mesarwi et al., 2021), liver fibrosis (Du et al., 2022) and liver cancer (Chen et al., 2023, Kou et al., 2023). Nevertheless, there is a limited number of reports investigating the regulatory role of these pathways in CCl_4-induced ALI. Further molecular docking and network analyses revealed that STW may play an important role in *S. chirayita* resistance to ALI. Particularly noteworthy, STW, is unique to the *Swertia* L. genus, which includes *S. chirayita* and *S. mussotii* (Guo et al., 2023). However, it has been relatively understudied in the context of CCl_4-induced ALI. Therefore, as a signature component of *Swertia* L., we have carried out further studies to highlight the important research value of STW.

A considerable amount of research has emphasized the role of inflammatory cytokines in the development of liver injury. It is possible that reducing these cytokines could potentially decrease the occurrence of diseases. Recent evidence suggests that TNF-α and IL-6 are particularly involved in experimental models of CCl_4-induced ALI (Zhang et al., 2016, Öztürk Akcora et al., 2017). Moreover, when the liver is exposed to high levels of CCl_4, the abnormal release of free radicals increases the permeability of cell membranes, leading to the infiltration of inflammatory neutrophils and the significant release of AST, ALT, IL-6, and TNF-α into the bloodstream, resulting in elevated serum levels. Consequently, the overexpression of ALT, AST, TNF-α, and IL-6 in the serum is considered a crucial indicator of ALI. The liver, which acts as the body's detoxifying organ, contains antioxidants such as SOD, MDA, glutathione peroxidase, and catalase. These antioxidants play a vital role in eliminating ROS and protecting the liver during alcohol metabolism (Dai et al., 2023). In this experiment, a 20-hour exposure to CCl_4 resulted in abnormal liver and serum expression of liver function markers (ALT and AST), inflammatory factors (IL-6 and TNF-α), and oxidative factors (MDA and SOD) in the model group. However, intervention with STW significantly reversed these abnormalities. Histopathological examination of the liver revealed a significant and dose-dependent improvement in cellular necrosis, inflammatory infiltration, and other liver tissue lesions after the STW intervention. It is important to note that the mechanism of these identified targets in CCl_4-induced ALI is not fully understood and requires further investigation. Previous studies have shown that targets such as EGFR, CASP3, and STAT3 are closely associated with diseases such as liver fibrosis (Wu et al., 2022), NASH (Peng et al., 2023), and ALI (Dai et al., 2023). However, the specific mechanisms of these targets in CCl_4-induced ALI are still unclear. The qRT-PCR results showed that STW significantly decreased the mRNA expression of key targets such as EGFR, CASP3, and STAT3, thereby relieving CCl_4-induced ALI. And molecular dynamics and immunohistochemistry further demonstrated the potential mechanism maybe related to ESR1 and MMP9. These findings corroborate the outcomes of our network pharmacological and molecular docking analyses, strengthening the hypothesis that STW plays a central role in *S. chirayita*'s medicinal effect on liver pathology.

However, our study has certain limitations and areas for improvement. Firstly, we focused only on the *in vitro* and blood components of the 80 % ethanol extract of *S. chirayita*. To provide more comprehensive experimental data, it would have been beneficial to conduct a comparative analysis of the chemical composition of ethanolic extracts at various concentrations. Secondly, although we used the UPLC-Q-Exactive Orbitrap MS technique for *ex vivo* compositional studies, it may have missed some trace components. Therefore, further investigations on the metabolites of *S. chirayita* are necessary. Additionally, our study only detected 10 prototypical blood components of *S. chirayita* using UPLC-Q-Exactive Orbitrap MS and did not consider the *in vivo* metabolism of these compounds. Thirdly, we only tested the compound STW, which had the highest docking score, against 10 core targets. To enhance the comprehensiveness of our study, it is important to conduct further in-depth research involving additional compounds and explore their protective activity in models. Finally, future investigations should focus on elucidating the mechanism of action of STW in intervening in CCl_4-induced ALI. This can be achieved through methodologies such as intestinal flora assessment, metabolomics, transcriptomics, plasmon resonance technology, and other tools, combined with *in vivo* validation in core gene-deficient mice.

While *S. Chirayita* and its key ingredient Swertiamarin have been traditionally used for treating liver diseases, our study offers several novel contributions to clinical practice. This includes the innovative application of systems biology approaches to systematically analyze the potential mechanisms of Swertiamarin in ALI, and the in-depth exploration of molecular mechanisms through network pharmacology and molecular docking. Furthermore, by providing experimental validation in the CCl4-induced ALI rat model, our study supports the clinical translation of Swertiamarin from a traditional remedy to a modern therapeutic agent. This highlights the multi-target nature of Swertiamarin, aligning with personalized medicine principles and suggesting potential for developing individualized treatment strategies for liver diseases.

5. Conclusions

In summary, UPLC-Q-Exactive Orbitrap MS, network pharmacology, and molecular docking techniques were utilized to analyze the bioactive compounds in *S. chirayita*. Additionally, *in vivo* experiments were conducted to investigate the mechanism of the active ingredient, STW, in ameliorating CCl_4-induced ALI. These results suggested that STW from *S. chirayita* may be the most crucial active substance for improving ALI. Furthermore, several key targets that play an important role in this process were identified, including EGFR, CASP3, CTNNB1, STAT3, SRC, ESR1, PTGS2, PPARG, TLR4, and MMP9, especially ESR1 and MMP9, and in addition, the PI3K/Akt, JAK/STAT, and HIF-1 pathways were considered as key pathways for its function. This research provides a solid theoretical framework for further exploration and development of *S. chirayita* and STW, paving the way for potential therapeutic applications.

6. Availability of data and materials

All data generated or analyzed during this study are included in this article.

CRediT authorship contribution statement

Sa Guo: Investigation, Methodology, Visualization, Writing – original draft. **Cen Wu:** Investigation, Methodology. **Xinwei Liu:** Investigation, Methodology. **Xianli Meng:** Writing – review & editing. **Yi Zhang:** Supervision, Writing – review & editing. **Shaohui Wang:** Conceptualization, Supervision, Writing – original draft, Writing – review & editing.

Declaration of competing interest

The authors declare that they have no known competing financial interests or personal relationships that could have appeared to influence the work reported in this paper.

Acknowledgement

This study was supported by the National Natural Science Foundation of China (81973573).

Appendix A. Supplementary data

Supplementary data to this article can be found online at https://doi.org/10.1016/j.arabjc.2024.105930.

References

Abdu, S., Juaid, N., Amin, A., et al., 2022. Effects of sorafenib and quercetin alone or in combination in treating hepatocellular carcinoma: in vitro and in vivo approaches. Molecules 27, 1–22. https://doi.org/10.3390/molecules27228082.

Amin, A., 2008. Ketoconazole-induced testicular damage in rats reduced by gentiana extract. Exp. Toxicol. Pathol. 59, 377–384. https://doi.org/10.1016/j.etp.2007.10.008.

Bekkouch, O., Dalli, M., Harnafi, M., et al., 2022. Ginger (Zingiber officinale Roscoe), Lemon (Citrus limon L.) Juices as preventive agents from chronic liver damage induced by CCl(4): a biochemical and histological study. Antioxidants (Basel) 11, 1–15. https://doi.org/10.3390/antiox11020390.

Bouabdallah, S., Al-Maktoum, A., Amin, A., 2023. Steroidal saponins: naturally occurring compounds as inhibitors of the hallmarks of cancer. Cancers 15, 3900. https://doi.org/10.3390/antiox11020390.

Chen, T., Wang, L., Chen, C., et al., 2023. HIF-1α-activated TMEM237 promotes hepatocellular carcinoma progression via the NPHP1/Pyk2/ERK pathway. Cell Mol. Life Sci. 80, 120. https://doi.org/10.1007/s00018-023-04767-y.

Chen, Q., Zhang, Y., Zhang, W., et al., 2011. Identification and quantification of oleanolic acid and ursolic acid in Chinese herbs by liquid chromatography-ion trap mass spectrometry. Biomed. Chromatogr. 25, 1381–1388. https://doi.org/10.1002/bmc.1614.

Chu, Q., Gu, X., Zheng, Q., et al., 2022. Regulatory mechanism of HIF-1α and its role in liver diseases: a narrative review. Ann. Transl. Med. 10, 109. https://doi.org/10.21037/atm-21-4222.

Dai, C., Zhang, X., Lin, J., et al., 2023. Nootkatone supplementation ameliorates carbon tetrachloride-induced acute liver injury via the inhibition of oxidative stress, NF-κB pathways, and the activation of Nrf2/HO-1 pathway. Antioxidants 12, 194. https://doi.org/10.3390/antiox12010194.

Deng, Z.P., Zhang, X., Tian, H.T., 2022. Identification of metabolites of isochlorogenic acid A in rats based on UHPLC-Q-Exactive Orbitrap MS. Shangdong Sci. 35, 1002–4026. https://doi.org/10.3976/j.issn.1002-4026.2022.06.008.

Di Paola, R., Modafferi, S., Siracusa, R., et al., 2022. S-acetyl-glutathione attenuates carbon tetrachloride-induced liver injury by modulating oxidative imbalance and inflammation. Int. J. Mol. Sci. 23, 4429. https://doi.org/10.3390/ijms23084429.

Dong, D., Zhang, S., Yin, L., et al., 2013. Protective effects of the total saponins from Rosa laevigata Michx fruit against carbon tetrachloride-induced acute liver injury in mice. Food Chem. Toxicol. 62, 120–130. https://doi.org/10.1016/j.fct.2013.08.050.

Du, Z., Huang, D., Shi, P., et al., 2022. Integrated chemical interpretation and network pharmacology analysis to reveal the anti-liver fibrosis effect of penthorum chinense. Front. Pharmacol. 13, 788388 https://doi.org/10.3389/fphar.2022.788388.

Du, Q., Xing, N., Guo, S., et al., 2023. Cycas revoluta leaves: as a potential flavonoids source for targeted regulation of immune-related markers in lung adenocarcinoma. Ind. Crops Prod. 202, 116967 https://doi.org/10.1016/j.indcrop.2023.116967.

Gawrieh, S., Chalasani, N., 2015. Pharmacotherapy for nonalcoholic fatty liver disease. Semin. Liver Dis. 35, 338–348. https://doi.org/10.1055/s-0035-1562951.

Gong, J., Chen, G.P., Li, L., et al., 2020. Analysis on chemical constituents of turkish galls by HPLC-ESI-IT-TOF- MS/MS. Tradit. Chin. Drug Res. Clin. Pharmacol. 31, 1227–1232. https://doi.org/10.19378/j.issn.1003-9783.2020.10.014.

Guan, J., Wang, L., Jin, J., et al., 2019. Simultaneous determination of calycosin-7-O-β-D-glucoside, cinnamic acid, paeoniflorin and albiflorin in rat plasma by UHPLC-MS/MS and its application to a pharmacokinetic study of Huangqi Guizhi Wuwu Decoction. J. Pharm. Biomed. Anal. 170, 1–7. https://doi.org/10.1016/j.jpba.2019.03.022.

Guo, S., Ouyang, H., Du, W., et al., 2021. Exploring the protective effect of Gynura procumbens against type 2 diabetes mellitus by network pharmacology and validation in C57BL/KsJ db/db mice. Food Funct. 12, 1732–1744. https://doi.org/10.1039/d0fo01188f.

Guo, S., Du, Q., Xing, N., et al., 2023. Swertia L.: a comprehensive review of its genetic relationship, chemical compositions, pharmacological effects, toxicities, and applications. Phytother. Res. 37, 2605–2643. https://doi.org/10.1002/ptr.7857.

Hamza, A.A., Mohamed, M.G., Lashin, F.M., et al., 2020. Dandelion prevents liver fibrosis, inflammatory response, and oxidative stress in rats. J. Basic Appl. Zool. 81, 43. https://doi.org/10.1186/s41936-020-00177-9.

He, X., Chen, M.H., Jin, L.L., et al., 2022. Progress in the chemical composition and pharmacological effects of chinese Swertia L. plants. Ginseng Res. 34, 45–53. https://doi.org/10.19403/j.cnki.16711521.2022.04.014.

Huang, B., Hu, Y.Z., Li, X., et al., 2021. Analysis of chemical constituents in odontosoria chinensis based on UPLC-Q-TOF-MS. Prac. Clin. J. Integr. Tradit. Chin. West Med. 21, 155–159. https://doi.org/10.13638/j.issn.1671-4040.2021.09.077.

Jaishree, V., Badami, S., 2010. Antioxidant and hepatoprotective effect of swertiamarin from enicostemma axillare against D-galactosamine induced acute liver damage in rats. J Ethnopharmacol. 130, 103–106. https://doi.org/10.1016/j.jep.2010.04.019.

Jia, L., Guo, H., Jia, B., et al., 2011. Anti-tumour activities and a high-performance liquid chromatography mass spectrometric method for analysis of the constituents of Lomatogonium carinthiacum. Nat. Prod. Res. 25, 100–107. https://doi.org/10.1080/14786419.2010.497146.

Kapoor, R., Huang, Y.S., 2006. Gamma linolenic acid: an antiinflammatory omega-6 fatty acid. Curr. Pharm. Biotechnol. 7, 531–534. https://doi.org/10.2174/138920106779116874.

Kim, S., Chen, J., Cheng, T., et al., 2023. PubChem 2023 update. Nucleic Acids Res. 51, D1373–D1380. https://doi.org/10.1093/nar/gkac956.

Kou, K., Li, S., Qiu, W., et al., 2023. Hypoxia-inducible factor 1α/IL-6 axis in activated hepatic stellate cells aggravates liver fibrosis. Biochem. Biophys. Res. Commun. 653, 21–30. https://doi.org/10.1016/j.bbrc.2023.02.032.

Kucharska, A.Z., Sokół-Łętowska, A., Oszmiański, J., et al., 2017. Iridoids, phenolic compounds and antioxidant activity of Edible Honeysuckle Berries (Lonicera caerulea var. kamtschatica Sevast.). Molecules 22, 405. https://doi.org/10.3390/molecules22030405.

Lin, Z., Aryal, S., Cheng, Y.H., et al., 2022. Integration of In vitro and in vivo models to predict cellular and tissue dosimetry of nanomaterials using physiologically based pharmacokinetic modeling. ACS Nano. 16, 19722–19754. https://doi.org/10.1021/acsnano.2c07312.

Liu, M., He, M., Gao, H., et al., 2019. Strategy for rapid screening of antioxidant and anti-inflammatory active ingredients in Gynura procumbens (Lour.) Merr. based on UHPLC-Q-TOF-MS/MS and characteristic ion filtration. Biomed. Chromatogr. 33, e4635.

Liu, X., Yu, Y., Wu, Y., et al., 2023. A systematic pharmacology-based in vivo study to reveal the effective mechanism of Yupingfeng in asthma treatment. Phytomedicine 114, 154783. https://doi.org/10.1016/j.phymed.2023.154783.

Mahendran, G., Thamotharan, G., Sengottuvelu, S., et al., 2014. Retracted: anti-diabetic activity of Swertia corymbosa (Griseb.) Wight ex C.B. Clarke aerial parts extract in streptozotocin induced diabetic rats. J. Ethnopharmacol. 151, 1175–1183. https://doi.org/10.1016/j.jep.2013.12.032.

Mao, Q., Cui, Y., Du, H., et al., 2022. San Pian decoction can treat nitroglycerin-induced migraine in rats by inhibiting the PI3K/AKT and MAPK signaling pathways. J. Ethnopharmacol. 296, 115470 https://doi.org/10.1016/j.jep.2022.115470.

Masuda, Y., 2006. Learning toxicology from carbon tetrachloride-induced hepatotoxicity. Yakugaku Zasshi. 126, 885–899. https://doi.org/10.1248/yakushi.126.885.

Mesarwi, O.A., Moya, E.A., Zhen, X., et al., 2021. Hepatocyte HIF-1 and intermittent hypoxia independently impact liver fibrosis in murine nonalcoholic fatty liver disease. Am J Respir Cell Mol Biol. 65, 390–402. https://doi.org/10.1165/rcmb.2020-0492OC.

Mou, J.J., Jin, C.Q., Liu, F., et al., 2020. Cleavage patterns of oxygen-substituted Xanthone analogues by electrospray mass spectrometry. Central South Pharmacy. 18, 953–958. https://doi.org/10.7539/j.issn.1672-2981.2020.06.010.

Niu, X., Liu, F., Li, W., et al., 2017. Hepatoprotective effect of fraxin against carbon tetrachloride-induced hepatotoxicity in vitro and in vivo through regulating hepatic antioxidant, inflammation response and the MAPK-NF-κB signaling pathway. Biomed Pharmacother. 95, 1091–1102. https://doi.org/10.1016/j.biopha.2017.09.029.

Öztürk Akcora, B., Storm, G., Prakash, J., et al., 2017. Tyrosine kinase inhibitor BIBF1120 ameliorates inflammation, angiogenesis and fibrosis in CCl(4)-induced liver fibrogenesis mouse model. Sci Rep. 7, 44545. https://doi.org/10.1038/srep44545.

Peng, C., Li, J., Ke, X., et al., 2023. In silico and in vivo demonstration of the regulatory mechanism of Qi-Ge decoction in treating NAFLD. Ann. Med. 55, 2200258. https://doi.org/10.1080/07853890.2023.2200258.

Swati, K., Bhatt, V., Sendri, N., et al., 2023. Swertia chirayita: a comprehensive review on traditional uses, phytochemistry, quality assessment and pharmacology. J. Ethnopharmacol. 300, 115714 https://doi.org/10.1016/j.jep.2022.115714.

Tan, Y., Huang, Z., Liu, Y., et al., 2023. Integrated serum pharmacochemistry, 16S rRNA sequencing and metabolomics to reveal the material basis and mechanism of Yinzhihuang granule against non-alcoholic fatty liver disease. J. Ethnopharmacol. 310, 116418 https://doi.org/10.1016/j.jep.2023.116418.

Tang, H., He, S., Zhang, X., et al., 2016. A network pharmacology approach to uncover the pharmacological mechanism of XuanHuSuo powder on osteoarthritis. Evid. Based Complement. Alternat. Med. 2016, 3246946. https://doi.org/10.1155/2016/3246946.

Tao, Y., Du, Y., Su, D., et al., 2017. UHPLC-MS/MS quantification combined with chemometrics for the comparative analysis of different batches of raw and wine-processed Dipsacus asper. J. Sep. Sci. 40, 1686–1693. https://doi.org/10.1002/jssc.201601459.

Terpinc, P., Cigić, B., Polak, T., et al., 2016. LC-MS analysis of phenolic compounds and antioxidant activity of buckwheat at different stages of malting. Food Chem. 210, 9–17. https://doi.org/10.1016/j.foodchem.2016.04.030.

Tian, J., Cai, M., Jin, S., et al., 2023. JianPi-QingHua formula attenuates nonalcoholic fatty liver disease by regulating the AMPK/SIRT1/NF-κB pathway in high-fat-diet-fed C57BL/6 mice. Pharm Biol. 61, 647–656. https://doi.org/10.1080/13880209.2023.2188549.

Tian, C., Zhang, T., Wang, L., et al., 2014. The hepatoprotective effect and chemical constituents of total iridoids and xanthones extracted from Swertia mussotii Franch. J. Ethnopharmacol. 154, 259–266. https://doi.org/10.1016/j.jep.2014.04.018.

Wang, D., Cai, T., Wu, Z.J., et al., 2016. LC-ESI-MS/MS analysis of chemical constituents in Yinhuang Qingfei capsule. China Meas. Test. 42, 36–40. https://doi.org/10.11857/j.issn.1674-5124.2016.03.009.

Wang, B., Cui, S., Mao, B., et al., 2022a. Cyanidin alleviated CCl_4-induced acute liver injury by regulating the Nrf2 and NF-κB signaling pathways. Antioxidants 11, 2383.

Wang, S., Du, Q., Sun, J., et al., 2022b. Investigation of the mechanism of Isobavachalcone in treating rheumatoid arthritis through a combination strategy of network pharmacology and experimental verification. J. Ethnopharmacol. 294, 115342 https://doi.org/10.1016/j.jep.2022.115342.

Wang, Q., Liu, J., Chen, X.L., et al., 2015. Study of the chemical composition of the white hairy silver dewberry based on the UPLC-Q-Orbitrap HRMS technique. J. Chin. Med. Mater. 43, 1901–1906. https://doi.org/10.19664/j.cnki.1002-2392.2015.05.021.

Wani, B.A., Ramamoorthy, D., Rather, M.A., et al., 2013. Induction of apoptosis in human pancreatic MiaPaCa-2 cells through the loss of mitochondrial membrane potential (ΔΨm) by Gentiana kurroo root extract and LC-ESI-MS analysis of its principal constituents. Phytomedicine 20, 723–733. https://doi.org/10.1016/j.phymed.2013.01.011.

Wu, Y., He, Y., Wang, R., et al., 2021. Preventive effect of flavonoid extract from the peel of Gonggan (Citrus reticulata Blanco Var. Gonggan) on CCl(4)-induced acute liver injury in mice. J. Inflamm. Res. 14, 5111–5121. https://doi.org/10.2147/jir.S332134.

Wu, B., Huang, L., Wang, Y., et al., 2022. Yao medicine Amydrium hainanense suppresses hepatic fibrosis by repressing hepatic stellate cell activation via STAT3 signaling. Front. Pharmacol. 13, 1043022. https://doi.org/10.3389/fphar.2022.1043022.

Xiao, G.L., Zhong, H.X., Huang, H.J., et al., 2022. Identification of chemical constituents in Xiao'er Qingyan granules by UPLC-Q-TOF-MS/MS. Chin. J. Mod. Appl. Pharm. 39, 1627–1636. https://doi.org/10.13748/j.cnki.issn1007-7693.2022.12.018.

Xie, Y., Mu, C., Kazybay, B., et al., 2021. Network pharmacology and experimental investigation of Rhizoma polygonati extract targeted kinase with herbzyme activity for potent drug delivery. Drug Deliv. 28, 2187–2197. https://doi.org/10.1080/10717544.2021.1977422.

Xin, C., Liu, S., Qu, H., et al., 2021. The novel nanocomplexes containing deoxycholic acid-grafted chitosan and oleanolic acid displays the hepatoprotective effect against CCl(4)-induced liver injury in vivo. Int. J. Biol. Macromol. 185, 338–349. https://doi.org/10.1016/j.ijbiomac.2021.06.109.

Xing, N., Qin, J., Ren, D., et al., 2023. Integrating UPLC-Q-Exactive Orbitrap/MS, network pharmacology and experimental validation to reveal the potential mechanism of Tibetan medicine Rhodiola granules in improving myocardial ischemia-reperfusion injury. J. Ethnopharmacol. 314, 116572 https://doi.org/10.1016/j.jep.2023.116572.

Xiong, R., Shan, S., Wang, X., et al., 2020. Aloperine attenuates carbon tetrachloride-induced mouse hepatic injury via Nrf2/HO-1 pathway. Trop. J. Pharm. Res. 19, 983–988. https://doi.org/10.4314/tjpr.v19i5.11.

Xu, J.P., Deng, J.G., Feng, Y.Q., 2008. Application of organic mass spectrometry to the structural identification of trace impurities in mangosteen APIs. J. Mass Spectrom. 29, 218–225, 1004-2997(2008)04-218-08.

Yang, Y., Yang, Y., Shen, Y., et al., 2023. Exploring the pharmacological mechanisms of Shuanghuanglian against T-cell acute lymphoblastic leukaemia through network pharmacology combined with molecular docking and experimental validation. Pharm. Biol. 61, 259–270. https://doi.org/10.1080/13880209.2023.2168703.

Zhan, J., Cao, H., Hu, T., et al., 2021. Efficient preparation of black tea extract (BTE) with the high content of theaflavin mono- and digallates and the protective effects of BTE on CCl(4)-induced rat liver and renal injury. J. Agric. Food Chem. 69, 5938–5947. https://doi.org/10.1021/acs.jafc.1c01851.

Zhang, G.L., 2021. Systematic characterization and quality evaluation of polybasic protogentian cyclic enol ether terpene components. Changchun University of Chinese Medicine, Changchun, 10.26980/d.cnki.gcczc.2021.000010.

Zhang, L., Cheng, Y., Du, X., et al., 2015. Swertianlarin, an herbal agent derived from Swertia mussotii Franch, attenuates liver injury, inflammation, and cholestasis in common bile duct-ligated rats. Evid. Based Complement. Alternat. Med. 2015, 948376 https://doi.org/10.1155/2015/948376.

Zhang, Z., Guo, M., Zhao, S., et al., 2016. ROS-JNK1/2-dependent activation of autophagy is required for the induction of anti-inflammatory effect of dihydroartemisinin in liver fibrosis. Free Radic. Biol. Med. 101, 272–283. https://doi.org/10.1016/j.freeradbiomed.2016.10.498.

Zhang, Y., Zhou, Q., Ding, X., et al., 2021. Chemical profile of Swertia mussotii Franch and its potential targets against liver fibrosis revealed by cross-platform metabolomics. J. Ethnopharmacol. 274, 114051 https://doi.org/10.1016/j.jep.2021.114051.

Zhao, X.T., Cao, D., Mao, W.L., et al., 2018. Analysis of chemical constituents of different polarity fractions from Liuwei Dihuang pills by HPLC. Tradit. Chin. Drug Res. Clin. Pharmacol. 29, 489–496. https://doi.org/10.19378/j.issn.1003-9783.2018.04.020.

Zheng, H.H., Luo, C.T., Chen, H., et al., 2014. Xanthones from Swertia mussotii as multitarget-directed antidiabetic agents. ChemMedChem. 9, 1374–1377. https://doi.org/10.1002/cmdc.201300507.

Zheng, W., Shi, H.Y., Wang, P., et al., 2022. Analysis of chemical constituents and blood-entry components of Hanxia Baijutsu Tianma Tang based on UPLC-Q-Orbitrap-HRMS technique. Chin. J. Hosp. Pharm. 42, 2331–2339. https://doi.org/10.13286/j.1001-5213.2022.22.04.